

RL-TR-91-317
Final Technical Report
December 1991

AD-A246 647



2

NONLINEAR OPTICS IN DENSE FREQUENCY NARROW SUPERSONIC BEAMS

Duke University

John E. Thomas

DTIC
ELECTE
FEB 25 1992
S D

APPROVED FOR PUBLIC RELEASE; DISTRIBUTION UNLIMITED.

92-03834



Rome Laboratory
Air Force Systems Command
Griffiss Air Force Base, NY 13441-5700

92 2 13 121

This report has been reviewed by the Rome Laboratory Public Affairs Division (PA) and is releasable to the National Technical Information Service (NTIS). At NTIS it will be releasable to the general public, including foreign nations.

RL-TR-91-317 has been reviewed and is approved for publication.

APPROVED: *Philip R. Hemmer*

PHILIP R. HEMMER
Project Engineer

FOR THE COMMANDER:

Harold Roth

HAROLD ROTH, Director
Solid State Sciences Directorate

If your address has changed or if you wish to be removed from the Rome Laboratory mailing list, or if the addressee is no longer employed by your organization, please notify Rome Laboratory (ERO) Hanscom AFB MA 01731-5000. This will assist us in maintaining a current mailing list.

Do not return copies of this report unless contractual obligations or notices on a specific document require that it be returned.

REPORT DOCUMENTATION PAGE

Form Approved
OMB No. 0704-0188

Public reporting burden for this collection of information is estimated to average 1 hour per response, including the time for reviewing instructions, searching existing data sources, gathering and maintaining the data needed, and completing and reviewing the collection of information. Send comments regarding this burden estimate or any other aspect of this collection of information, including suggestions for reducing this burden, to Washington Headquarters Services, Directorate for Information Operations and Reports, 1215 Jefferson Davis Highway, Suite 1204, Arlington, VA 22202-4302, and to the Office of Management and Budget, Paperwork Reduction Project (0704-0188), Washington, DC 20503.

1. AGENCY USE ONLY (Leave Blank)		2. REPORT DATE December 1991		3. REPORT TYPE AND DATES COVERED Final Apr 88 - Dec 90	
4. TITLE AND SUBTITLE NONLINEAR OPTICS IN DENSE FREQUENCY NARROW SUPERSONIC BEAMS				5. FUNDING NUMBERS C - F19628-88-K-0012 PE - 61102F PR - 2305 TA - J7 WU - 34	
6. AUTHOR(S) John E. Thomas					
7. PERFORMING ORGANIZATION NAME(S) AND ADDRESS(ES) Duke University Office of Research Support Durham, Durham County, NC 27706				8. PERFORMING ORGANIZATION REPORT NUMBER N/A	
9. SPONSORING/MONITORING AGENCY NAME(S) AND ADDRESS(ES) Rome Laboratory (ERO) Hanscom AFB MA 01731-5000				10. SPONSORING/MONITORING AGENCY REPORT NUMBER RL-TR-91-317	
11. SUPPLEMENTARY NOTES Rome Laboratory Project Engineer: Philip R. Hemmer/ERO/(617) 377-5170					
12a. DISTRIBUTION/AVAILABILITY STATEMENT Approved for public release; distribution unlimited.				12b. DISTRIBUTION CODE	
13. ABSTRACT (Maximum 200 words) A broad program of research has been undertaken to develop novel magnetically compensated supersonic beams and to study the interaction of light with these systems. The technique was demonstrated initially with strontium where a 50% absorption and 18 MHz linewidth was obtained using a transition with a 22 usec radiative lifetime. The new method was then applied to observe continuous spatial photon echoes in samarium, which will have important applications in spatial phase conjugation and in nonlinear optical processing including optical field spatial convolution and correlation. In addition to this research, the use of a magnetic field gradient in the magnetic compensation method led to the development of novel Raman induced resonance imaging techniques for moving atoms in beams. The method can achieve uncertainty limited spatial resolution in the nanometer region with wide applications in atomic optics, including interferometers, gyroscopes and ultrahigh resolution lithography.					
14. SUBJECT TERMS Nonlinear optics, Atomic beams, Raman scattering, Photon echoes				15. NUMBER OF PAGES 40	
				16. PRICE CODE	
17. SECURITY CLASSIFICATION OF REPORT UNCLASSIFIED	18. SECURITY CLASSIFICATION OF THIS PAGE UNCLASSIFIED	19. SECURITY CLASSIFICATION OF ABSTRACT UNCLASSIFIED	20. LIMITATION OF ABSTRACT UL		

NSN 7540-01-280-8000

Standard Form 298 (Rev. 2-89)
Prescribed by ANSI Std. Z39-18
298-102

Accession For	
NTIS	CRA&I <input checked="" type="checkbox"/>
DTIC	TAB <input type="checkbox"/>
Unannounced <input type="checkbox"/>	
Justification	
By	
Distribution /	
Availability Code	
Dist	Avail and/or Special
A-1	

I. DEMONSTRATION OF MAGNETICALLY COMPENSATED SUPERSONIC BEAMS

The first step in our program was to demonstrate that the magnetically compensated supersonic beam was a viable concept, by achieving a very large single pass absorption coefficient and narrow linewidth in a weak atomic transition. Briefly, the compensated beam system consists of a tantalum tube oven, filled partially with the atomic metal of interest, and heated by a current of up to 500 A. Drilled in the side of the tube is a pinhole of 50–150 microns diameter through which a supersonic atomic beam emerges after adiabatic expansion. This beam has the narrow spread of thermal speed due to the cooling effect of the expansion. A laser beam intersects the atomic beam at right angles to the central axis of the emerging cone of atoms. In the absence of any magnetic compensation, atoms which travel at different angles with respect to the laser beam experience different Doppler shifts. In this case, the absorption linewidth for an interaction path length of 4.4 cm is about 500 MHz for a typical visible transition. The interaction is limited to those atoms which are Doppler shifted within a natural linewidth (or transit width) of resonance. In order to dramatically increase the number of interacting atoms, a pair of opposing magnet coils is placed on the laser beam axis on either side of interaction region. For the atomic transitions employed in the experiments, which are all $J = 0$ ground state to $J = 1, M = 1$ excited state optical transitions, the magnet coils have the effect of producing a field gradient which shifts the excited state as a function of the atomic position along the laser axis. Since the Doppler shift varies approximately linearly in position along the laser beam axis, the strength of the magnetic field gradient generated by the opposing magnet coils can be adjusted to cancel the Doppler shift over an extended region along the laser beam axis. This leads to a very narrow resonance line and tremendously enhanced absorption which is ideal for nonlinear optics experiments.

This method was demonstrated initially using the $^1S_0 \rightarrow ^3P_1$ transition in ^{174}Yb at 556 nm. With a radiative lifetime of 875 ns, the absorption coefficient for a weak laser beam traversing a 4.4 cm path of atoms was so large that it did not go below 50% until the laser was detuned more than 50 MHz from resonance.

In order to carefully study the lineshape for the magnetically compensated beam, it was realized that a much weaker transition was needed. For this purpose, the $^1S_0 \rightarrow ^3P_1$ transition in ^{88}Sr at 690 nm was selected. With a radiative lifetime of 22 μsec , this transition seemed ideal for the study, and opened up the possibility of coherent interaction of the atomic system with the laser field over extended distance along the atomic beam axis. Unfortunately, operation of the ring dye laser at this

wavelength proved to be a formidable task. Pyridine 2 optics were used with Pyridine 1 dye. When these were installed in the 699-21 dye laser, it was not possible to obtain lasing. This resulted in a substantial time loss. Finally, we inserted a 100% reflector in the laser output port and converted to standing wave operation. Once the initial alignment was completed, a 4% output coupler was inserted and 500 mW at 690 nm was obtained open cavity using 6 W of all lines argon ion pump power. By using a 2% output coupler, we finally obtained 100 mW of stable single mode power with only 5 W of pump power, which enabled us to begin the lineshape experiments in strontium.

The data obtained in the strontium experiments demonstrated beautifully the magnetically compensated beam method and yielded good lineshapes which could be compared to predictions. An absorption enhancement of 29:1 was obtained with the compensating coils to achieve a 50% absorption and a compensated linewidth of 18 MHz. The atomic density in the 4.4 cm interaction path was estimated at 1.2×10^{11} . The lineshapes obtained were in good agreement with theoretical predictions which included the frequency chirping due to the atomic motion across the magnetic field gradient.

Publications based on this Research

1) K.D. Stokes, C. Schnurr, J. Gardner, M. Marable, S. Shaw, M. Goforth, D.E. Holmgren, and J. E. Thomas, "Magnetically Compensated Supersonic Beams for Nonlinear Optics," *Optics Letters* 14, 1326 (1989).

II. CONTINUOUS SPATIAL PHOTON ECHOES

In demonstrating the magnetic compensation method in atomic strontium, it was appreciated that the long radiative lifetime of the 3P excited electronic state opened up the possibility of achieving continuous coherent interaction of the atomic system with laser fields over large distances along the atomic beam axis. One important application is the development of continuous spatial photon echoes in atomic beams. Continuous echoes can be used for nonlinear optical processing, including spatial phase conjugation and correlation or convolution of pairs of optical fields. In addition, continuous generation of dense macroscopic optical coherence in atomic beams has applications in a variety of fundamental experiments, such the evolution of optical coherence in cavities, and the study of optical quantum noise.

Due to the difficulty we experienced in the strontium experiments, we sought a different atomic system for the echo experiments. The appropriate system needed a simple two level atomic transition in the visible region with a somewhat longer spontaneous lifetime than ytterbium. After some searching, the samarium atomic system presented itself as a good choice. For the first experiments, the $^7F_0 \rightarrow ^7D_1$ transition at 599 nm was chosen. With a 1.7 μ sec radiative lifetime, it permitted coherence to propagate over millimeter distances along the atomic beam axis. Further, the transition permitted the use of R6G dye, greatly simplifying the dye laser operation.

In the experiments, the atomic beam is magnetically compensated by taking advantage of the excited state Zeeman tuning, for which the g-factor is 2.83. For a 1 cm interaction path length with the laser fields, the Doppler width without compensation, 100 MHz, is reduced to 5 MHz. The atoms cross two *cw* focussed laser beam regions, each of 50 micron diameter. This yields a transit time bandwidth somewhat larger than the compensated Doppler width. In this way, nearly all atoms interact strongly with the laser fields. The field intensities were adjusted to yield nominally $\pi/2$ and π pulse areas in the atom frame, to optimize the echo amplitude. With the laser fields separated by 0.5 mm, a strong continuous echo field was observed 1 mm downstream from the first laser field. Unlike previous work on continuous coherent radiation by atoms which traverse separated fields, the echo fields generated in the present experiments could be viewed with the unaided eye. Prior work utilized heterodyne beats with a strong local oscillator to make measurements. A permanent record of the spatial echo signals in our experiments was obtained by imaging the echo field onto a Reticon diode array.

The measurements yielded a somewhat unexpected nonexponential decay characteristic for the spatial echo signal as a function of separation between the input laser fields. This was found to be due to the magnetic compensation, which causes the atomic radiation frequency to chirp as the atoms move through the field gradient. A simple theory taking the chirp effect into account yielded predictions in qualitative agreement with the data.

The experiments demonstrated that very dense optical coherence can be generated and transported downstream in a magnetically compensated beam. This method opens up the possibility of a variety of fundamental and applied physics experiments as discussed above.

Publications based on this Research

- 1) C. Schnurr, K.D. Stokes, G.R. Welch, and J.E. Thomas, "Continuous Spatial Pho-

ton Echoes." Optics Letters 15, 1098 (1990).

2) J.E. Thomas, K.D. Stokes, C. Schnurr, and G.R. Welch, "Continuous Spatial Photon Echoes," IQEC '90 (Anaheim, May 1990).

III. PRECISION ATOMIC POSITION MEASUREMENT USING OPTICAL FIELDS

The success in applying magnetic field gradients to compensating the Doppler broadening of diverging supersonic beams suggested that it might be fruitful to pursue other applications of field gradients. Motivated by the lack of position measurement techniques for *moving* atoms in atomic beams, we have developed a novel atomic imaging technique based on resonance imaging in intense field gradients. The purpose of the methods which are being developed is to replace the mechanical hot wire and slit methods generally used for measuring atomic beam intensity distributions with high resolution optical techniques. It is expected that the new techniques, which ultimately can achieve *uncertainty limited* position resolution in the nanometer region, will find wide applications in the newly emerging field of atomic de Broglie optics.

The basic method is use a spatially varying potential to make the resonance frequency of simple atoms position dependent, analogous to magnetic resonance (MR) imaging. Unlike conventional MR imaging, the method employs Raman- induced resonance imaging using optical fields. The use of optical fields permits the measurements to be made in very small volumes with very large spatially varying potentials. This leads to quantum mechanical limits on the measurement accuracy.

In the initial experiments, an atomic samarium beam is collimated to 1 mm and passes through three regions:

i) An optical pumping beam, resonant on the ${}^7F_1 \rightarrow {}^7F_0$ transition at 571 nm. This beam empties the $M = 1$ sublevel of the 7F_1 electronic ground fine structure state, leaving population in the $M = 0$ sublevel. This level is used as the initial state for a Raman transition back to the $M = 1$ sublevel.

ii) A Raman region containing two optical fields, both of which are 100 MHz off resonant with the 7F_0 excited state. This region induces Raman transitions from the $M = 0$ initial state to the $M = 1$ final state, which is initially empty. In this region, a 100 G uniform magnetic field plus a 500 G/cm field gradient are applied. The net effect of these two fields is to shift the $M = 1$ ground sublevel at a rate of 10^9 Hz/cm. The optical Raman fields are generated by acoustooptic modulation

from a common laser field to eliminate laser jitter and achieve transit time limited frequency resolution on the Raman transition. With an atomic beam speed of 8.6×10^4 cm/sec and a Raman region diameter of 2.3 mm, transit limited resolution of 230 kHz (FWHM) is predicted and obtained in the experiments when the gradient magnet is off.

With the gradient magnet on, only atoms in the spatial region tuned within 230 kHz of resonance with the Raman fields make a Raman transition from the initial $M = 0$ state to the final $M = 1$ state.

iii) An optical field resonant with the 7F_1 , $M = 1 \rightarrow {}^7F_0$ interrogates the $M = 1$ final state. The number of atoms in the final state is proportional to the number of atoms in the initial state near the spatial region where resonance with the Raman fields occurs. By measuring resonance fluorescence intensity in this region as a function of the uniform magnetic field strength, the spatial region resonant with the Raman fields is swept across the atomic distribution, yielding the atomic density as a function of position across the atomic beam.

At present, spatial resolution has been studied by measuring the shadow of a 25 micron diameter gold coated tungsten wire placed just before the Raman fields. To date, the best resolution is about 2.5 microns, which is close to the theoretical limit of 1.7 microns due to the velocity of the moving atoms along the measurement axis.

Much higher resolution will be obtained with the next generation systems which employ large spatially varying light shifts instead of magnetic field gradients. This method permits final state tuning rates of 10^{12} Hz/cm over micron regions. Since the initial state is *not* shifted by the applied spatially varying potential, momentum is imparted to the atom only after it makes a transition into the final state. In this case, for adequately collimated atomic beams ($50 \mu\text{r}$ half angle) it is easy to show that the momentum spread imparted by the force due to the field gradient and the position resolution obey the Heisenberg uncertainty relation. In fact, for a Raman region comprised of laser beams with a gaussian spatial intensity distribution, it is possible to put atoms into the final state in a gaussian minimum uncertainty wave packet.

Publications based on this Research

- 1) J.E. Thomas, "Uncertainty-Limited Position Measurement of Moving Atoms using Optical Fields," Optics Letters 14, 1186 (1989).

- 2) J.E. Thomas, "Quantum Theory of Atomic Position Measurement using Optical Fields," Phys. Rev. A **42**, 5652 (1990).
- 3) J.E. Thomas, K.D. Stokes, C. Schnurr, J. Gardner, and G.R. Welch, "Atomic Position Measurement and Localization using Optical Fields," De Broglie Optics Workshop, (Santa Fe, N.M. 1990).
- 4) G.R. Welch, K.D. Stokes, C. Schnurr, J. Gardner, and J.E. Thomas, "Uncertainty Limited Atomic Position Measurement using Optical Fields," Symposium on Atomic Optics, Annual Meeting of the Optical Society of America, Boston, MA (November, 1990).

Report of Inventions based on this Research

- 1) Precision Optical Measuring System for Atoms in Beams
(submitted to Duke office of Technology Transfer, file #00635)

Magnetically compensated supersonic beams for nonlinear optics

K. D. Stokes, C. Schnurr, J. Gardner, M. Marable, S. Shaw, M. Goforth, D. E. Holmgren, and J. E. Thomas

Department of Physics, Duke University, Durham, North Carolina 27706

Received July 12, 1989; accepted September 25, 1989

Doppler frequently shifts for a laser field interacting with a diverging supersonic atomic beam are canceled using spatially varying Zeeman shifts. Dense atomic beams with long interaction path lengths and narrow linewidths are obtained for spectroscopic and nonlinear-optics applications.

It is well known that supersonic beams are useful for producing dense sources of atoms and molecules for spectroscopic applications.^{1,2} In such beams, adiabatic expansion causes the temperature to drop so that the velocity distribution relative to the average stream speed is narrow.^{1,2} This low-temperature characteristic has been exploited in a variety of experiments to produce weakly bound species, such as van der Waals's molecules,³ and to produce clusters.⁴ For optical laser spectroscopy, however, the wide divergence angle of the expanding beam leads to substantial Doppler broadening, which is reduced in many experiments by collimation. Collimation is adequate whenever the signal-to-background ratio or experimental requirements permit a short interaction path length. In many experiments this is not the case, and alternative means of reducing the linewidth have been developed. Recently, pulsed slit nozzles have been used to reduce Doppler broadening of a long-path-length (2.5-cm) molecular beam by exploiting the fact that the streamlines of the beam tend to be perpendicular to the slit except at the edges.⁵ Linewidth reductions of threefold to sixfold in infrared spectra have been obtained in this way.⁵ While this technique is general, the slit configuration requires pulsed operation to reduce source consumption and pumping requirements. Furthermore, the linewidth reduction is modest for some applications.

In nonlinear-optics applications, it is often important to have a high-density beam and a long interaction path with a narrow linewidth in the optical region. In this Letter a new technique is demonstrated that achieves this goal by using a spatially varying Zeeman shift to compensate the Doppler broadening of a diverging supersonic beam.⁶ A greater than 20-fold linewidth reduction and peak absorption enhancement are obtained on the $^1S_0 \rightarrow ^3P_1$ transition at 690 nm in ^{88}Sr , for which the radiative lifetime is 22.4 μsec . Absorptions of greater than 50% and a linewidth of ~ 18 MHz are obtained with a 4.4-cm interaction path length.

The $^1S_0 \rightarrow ^3P_1$ transition at 690 nm in ^{88}Sr was chosen for the demonstration because of its long 22.4- μsec radiative lifetime and correspondingly weak transition strength. In this way, the compensated line

shape can be accurately studied at high density and long path length without the sample's becoming optically thick.

The basic features of the compensated beam system are shown in Fig. 1. A tantalum oven is heated with a few hundred amperes of ac current to obtain a high density of active species. A supersonic beam emerges from a 150- μm pinhole nozzle drilled in the side of the tantalum tube and passes through a 2.5-cm aperture located 8 cm downstream from the nozzle. The corresponding divergence half-angle is 0.156 rad. The species chosen for study, Sr and Yb, have two valence electrons and negligible dimer formation. Hence, no carrier gas is needed for the experiments, and, since the metals are condensable, only a small, 5-cm (2-in.) diffusion pump is used for the vacuum system. A circularly polarized laser beam of ~ 0.5 -mm $1/e$ intensity radius crosses the atomic beam 14 cm from the nozzle so that the interaction path length is 4.4 cm. In this case, taking the laser beam propagation direction as the quantization z axis, the $J = 0, M = 0 \rightarrow J = 1, M$

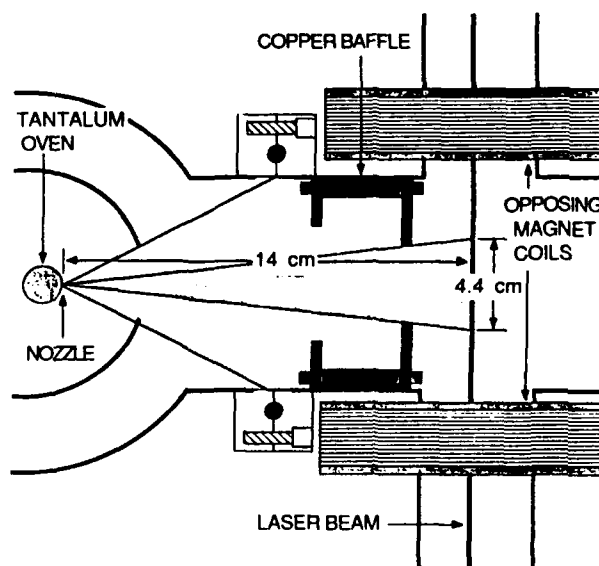


Fig. 1. Magnetically compensated supersonic beam.

= 1 transition at 690 nm is excited. Without magnetic compensation, the Doppler-broadened linewidth for this configuration is found to be ~480 MHz.

To reduce the Doppler linewidth, we exploit the low-temperature narrow velocity distribution of the supersonic beam.^{1,2} In this case, the Doppler frequency shift of a given atom is approximately $v_0\theta/\lambda$, where v_0 is the average stream speed, θ is the angle between the atom direction of motion and the perpendicular to the laser beam, and λ is the optical wavelength. Since θ is approximately linear in distance along the laser beam axis, the Doppler frequency shift is also approximately linear with position along the laser axis. Hence, a spatially varying Zeeman shift can be used to tune each atom into resonance with the local Doppler-shifted laser frequency, so that the entire interaction length of the atomic beam can be made to resonate at the same frequency. The field produced by a pair of opposing magnet coils (Fig. 1) is used to Zeeman tune the $M = 1$ excited state, for which the g factor is $3/2$. The aspect ratio for these coils is chosen for maximum field gradient, and the coils are water cooled. In a typical experiment the gradient required to compensate the Doppler broadening is only approximately 50 G/cm for the Zeeman tuning rate of 2 MHz/G.

Figure 2 shows the absorption enhancement and line narrowing obtained using magnetic compensation compared with that obtained without compensation. In this case, the maximum linear absorption is limited to 50% in order to investigate the line shape. Absorptions up to ~80% were obtained in this system at higher oven temperatures. With the present setup, nozzle clogging often occurred at still higher oven temperatures when Sr was used as the active species, although this did not happen for Yb.

In order to understand the line shape for the compensated beam, the *path-averaged* linear absorption coefficient was calculated in first-order perturbation theory. The result is easily understood using heuristic arguments and is given by

$$\alpha(\Delta) = n_0 \frac{4\pi^2 k \mu^2}{h} \int_{-\theta_{\text{MAX}}}^{\theta_{\text{MAX}}} \frac{d\theta}{2\theta_{\text{MAX}}} \exp \left\{ - \frac{\left[\Delta - \left(q - \beta \frac{y_1}{v_0} \right) v_0 \theta \right]^2}{\Gamma^2(\theta)} \right\} \times \frac{1}{\Gamma(\theta) \sqrt{\pi}}, \quad (1)$$

where Δ is the laser detuning and the angle-dependent linewidth is given by

$$\Gamma(\theta) = \left\{ \frac{v_0^2}{R^2} + (\beta r_0)^2 + [(\beta R)^2 + (qu)^2] \theta^2 \right\}^{1/2}. \quad (2)$$

The laser beam centered at a distance from the source, y_1 , has an intensity $1/e$ radius R and a wave vector q . The supersonic atomic speed distribution is assumed to be a Gaussian of $1/e$ width u relative to the mean speed v_0 . It is assumed also that the atomic density does not vary across the interaction path length for the small angles of interest here. This is consistent with the flatness of the experimental un-

compensated absorption line shape that effectively measures the atomic spatial distribution. The Zeeman tuning rate per centimeter is $\beta \equiv (g\mu_B/h)(\partial B_0/\partial z)$.

Gaussian velocity and starting position distributions are assumed, so that the line shape in Eq. (2) is a sum of Gaussian line shapes for each angle θ . The spontaneous linewidth is considered negligible compared to other sources of line broadening. With the above definitions, primary contributions to the linewidth arise from the laser beam transit rate v_0/R and from the variation of the Zeeman shift due to the distribution of the starting positions of atoms across the oven nozzle, which is taken to be a Gaussian of $1/e$ width r_0 . For a point source this contribution vanishes. Angle-dependent contributions to the linewidth arise from the Zeeman frequency chirp $\beta R\theta$ as atoms move across the laser beam and from the longitudinal residual Doppler width $qu\theta$, which results from the projection of the width of the speed distribution onto the laser beam propagation direction. Note that for a given speed the Doppler frequency shifts corresponding to different angles θ are included in the analysis through the uniform angular distribution. These Doppler shifts are compensated by the magnetic field gradient. The frequency-integrated absorption coefficient is just the usual two-level atom result $n_0(4\pi^2 k \mu^2/h) = (\pi/2)\gamma_{\text{spont}}\sigma_{\text{opt}}n_0$, where $\sigma_{\text{opt}} = (3/2\pi)\lambda^2$ and n_0 is the ^{88}Sr atomic density in the interaction region. For an interaction path length l , the measured weak field transmitted power fraction will be $\exp[-\alpha(\Delta)l]$.

To compare the calculated and experimentally observed absorption line shapes, input parameters were calculated for the measured oven temperature of ~1100°C using standard one-dimensional adiabatic expansion results.^{1,2} The total oven density is estimated from the vapor pressure curve⁷ to be $n = 70.2 \times 10^{16}/\text{cc}$. The corresponding stream speed is $v_0 = 1.3 \times 10^5 \text{ cm/sec}$. Assuming a collision cross section of 60 \AA^2 and a collision effectiveness of 0.25, one obtains a terminal Mach number of 6.2 and a velocity spread of

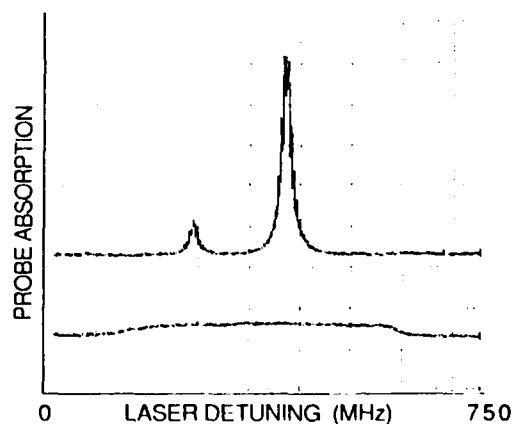


Fig. 2. Uncompensated (lower trace) and compensated (upper trace) absorption line shapes in Sr. The maximum compensated absorption is 50%. The larger (smaller) peak is the ^{88}Sr (^{86}Sr) isotope.

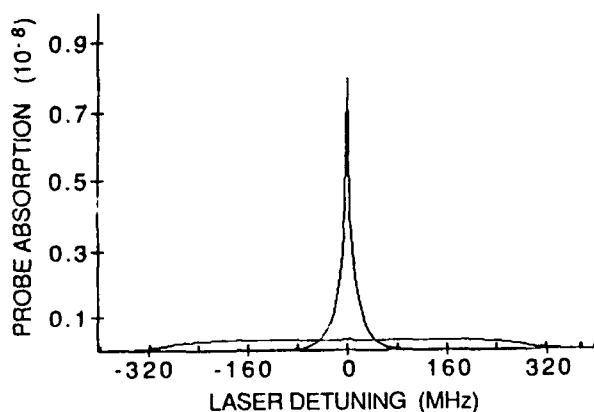


Fig. 3. Theoretical compensated and uncompensated absorption coefficients versus the detuning in units of $\alpha_0 = 4\pi^2 k \mu^2 n_0 / h$.

$u = 2.3 \times 10^4$ cm/sec.² These numbers yield a residual Doppler shift of $qu = 2.1 \times 10^9$ rad/sec per radian and an uncompensated Doppler line broadening of $qu_0 = 1.2 \times 10^{10}$ rad/sec per radian. For $y_1 = 14$ cm the optimum Zeeman shift per unit length is $\beta = qu_0/y_1 = 0.84 \times 10^9$ rad/sec per centimeter. With a laser beam of 0.5-mm intensity $1/e$ radius, the frequency chirp per radian is $\beta R = 0.42 \times 10^8$ rad/sec, which is negligible compared to the residual Doppler shift per radian. Since the spontaneous lifetime is long, the primary contribution to the angle-independent linewidth arises from the oven aperture and the compensating field gradient. For a nozzle radius of $r_0 = 75$ μ m, this linewidth is $\beta r_0 = 0.56 \times 10^7$ rad/sec. With the compensating field off, the corresponding linewidth is transit time limited with $v_0/R = 0.26 \times 10^7$ rad/sec for a laser beam intensity $1/e$ radius of 0.5 mm. Using these parameters, one obtains the results shown in Fig. 3.

The maximum calculated absorption at line center can be used to estimate the atomic density, which is $0.8 \times 10^{-8} (\pi/2) \gamma_{\text{spont}} \sigma_{\text{opt}} n_0$. For the measured 50% absorption, one can estimate the atomic density using $\alpha l = 0.69$, $l = 4.4$ cm, $\sigma_{\text{opt}} = 2.3 \times 10^{-9}$ cm² at 690 nm, and $\gamma_{\text{spont}} = 4.46 \times 10^4$ sec⁻¹. This yields $n_0 = 1.2 \times 10^{11}$ /cc. For comparison, the total Sr density calculated from the oven density at a distance $L = 14$ cm from the nozzle (assuming that the atoms travel in straight lines after the adiabatic expansion ends) is $0.157(2r_0/L)^2 n = 1.27 \times 10^{11.2}$. Using the ⁸⁸Sr abundance of 83%, we have $n_0 = 1.05 \times 10^{11}$.

The calculated ratio of peak compensated to uncompensated absorption is 29.0:1, which compares well with the measured value of 29:4:1. Note that in the Doppler-broadened limit, collimation of an uncompensated beam will reduce the linewidth without changing the uncompensated absorption. Hence, the improvement over a collimated atomic beam with the same source consumption and linewidth is roughly of a factor of 29. Higher absorption coefficients and narrower linewidths can be obtained at a higher source density. However, collisions outside the nozzle ulti-

mately increase the effective source size and thereby increase the linewidth.

While the calculated compensation ratio and density agree well with the experimental values, the line shape obtained using the parameters based on the oven temperature and oven diameter is qualitatively different from that measured. Better agreement is obtained by enlarging the effective nozzle diameter by a factor of 6 to take into account collisions in the expansion region, thus increasing the angle-independent linewidth. The residual Doppler width is then reduced by assuming a higher Mach number of 12.4 (a larger collision cross section). This decreases the pedestal on the calculated line shape, and the HWHM can be made to agree with the experimentally observed value of approximately 18 MHz. Since parameters are chosen to obtain agreement with the compensated and uncompensated maximum absorption at line center, the calculated atomic density obtained in the interaction region remains as stated above.

The compensated beam system demonstrated here provides a reasonably general technique for obtaining high atomic densities and long interaction path lengths for nonlinear optics and spectroscopic experiments while a narrow linewidth is maintained. It can be applied whenever the Doppler shift and the position are correlated. In addition to supersonic beams, any type of accelerated beam, for which the fractional velocity spread is small, can be compensated to reduce the spectral linewidth. We have applied the compensated beam technique to the $^1S_0 \rightarrow ^3P_1$ transition of ¹⁷⁴Yb, where the sample was easily made optically thick although the spontaneous lifetime is 875 nsec. While this technique is effective for only one M level and propagation direction, it may have important applications to atom-cavity experiments requiring a high atomic density of two-level atoms and to nonlinear-optics experiments in general. In addition, for weak-line spectroscopy, this method may provide a means of obtaining substantial signal enhancement.

This research is supported by the Rome Air Development Center under contract F19628-88-K-0012.

References

1. A. Kantrowitz and J. Grey, *Rev. Sci. Instrum.* **22**, 328 (1950).
2. J. B. Anderson and J. B. Fenn, *Phys. Fluids* **8**, 780 (1964).
3. See, e.g., R. A. Gottcho, R. A. Bitar, W. P. Lapatovich, I. Renhorn, and D. E. Pritchard, *J. Chem. Phys.* **75**, 2546 (1981).
4. See, e.g., T. G. Dietz, M. A. Duncan, D. E. Powers, and R. E. Smalley, *J. Chem. Phys.* **74**, 6511 (1981), and references therein.
5. C. M. Lovejoy and D. J. Nesbitt, *Rev. Sci. Instrum.* **58**, 807 (1987); C. M. Lovejoy, M. D. Schuder, and D. M. Nesbitt, *J. Chem. Phys.* **85**, 4890 (1986).
6. A prototype of this system was demonstrated previously by D. J. Heinzen, J. E. Thomas, and M. S. Feld at the MIT Spectroscopy Laboratory, Cambridge, Massachusetts.
7. *CRC Handbook of Chemistry and Physics*, 68th ed. (CRC Press, Boca Raton, Fla., 1987).

Continuous spatial photon echoes

C. Schnurr, K. D. Stokes, G. R. Welch, and J. E. Thomas

Department of Physics, Duke University, Durham, North Carolina 27706

Received April 30, 1990; accepted July 30, 1990

We report the observation of continuous spatial photon echoes in a magnetically compensated supersonic beam of atomic samarium. Atoms cross two spatially separated cw laser pump fields to produce an intense cw echo downstream. In contrast to previous studies of continuous coherent radiation in separated fields, the signals are readily observable with the unaided eye. The echo signal, which is generated in a magnetic-field gradient, differs from usual rephasing phenomena owing to a quadratic time dependence for the optical phase in the frame of the moving atoms.

Since the first observation of the photon echo,¹ optical rephasing techniques have found a variety of applications in studies of relaxation phenomena in vapors and condensed-matter systems. Recently, rephasing techniques have been applied to optical processing² and information storage.³⁻⁵ Rephasing techniques also have found important application in developing optical Ramsey resonance techniques in atomic beams.⁶

In this Letter we report the observation of a new type of continuous spatial photon echo in a magnetically compensated supersonic beam⁷ of samarium atoms. By using a magnetic-field gradient to compensate the Doppler shifts of the diverging supersonic beam, a high product of density and path length (nl) is obtained. In this case, substantial optical coherence is spatially transferred in the experiments, leading to large coherent signals that are radiated and directly detected downstream from two pump regions that the atoms traverse. Continuous coherent radiation by atoms that have traversed spatially separated pump fields leads to signals proportional to the square of the number of atoms and so is closely related to superradiance in extended media.⁸ Coherent radiation in separated fields has been studied previously in vapors⁹ without the use of a magnetically compensated beam. However, heterodyne detection was needed to measure the 10^{-15} -W signals that were obtained.

In our experiments (Fig. 1) a supersonic atomic beam traverses two continuous pump regions. These regions play the roles of the usual $\pi/2$ and π pulses in temporal rephasing phenomena as seen in the atom frame. Hence, inhomogeneous dephasing of the macroscopic polarization during the traversal time between the two pump beams is reversed after the second pump field, leading to a large macroscopic polarization downstream from the second pump region. This idea has been exploited previously in three-beam optical Ramsey resonance experiments to eliminate optical dephasing.⁶ Unlike that in previous experiments, which measure a small absorption or fluorescence, our system employs a magnetically compensated supersonic beam to achieve a long interaction path length in the medium with a narrow Doppler band-

width. This permits a large optical polarization to be obtained so that the echo field generated by the atomic medium 0.5 mm downstream from the pump region is visible with the unaided eye, in contrast to previous experiments on continuous radiation in spatially separated fields.⁹

The system employs a supersonic samarium beam that emerges from a 150- μ m pinhole drilled in the side of an electrically heated tantalum tube. This beam is collimated to a 1-cm aperture, where it crosses two cw linearly polarized pump fields of powers of a few hundred microwatts. Using a 50- μ m waist and a 2-mm height for the pump beams, we achieve a transit time bandwidth of 5 MHz. The $^7F_0 \rightarrow ^7D_1$ transition at 599 nm is excited for which the radiative lifetime is 1.7 μ sec. Without magnetic compensation, the Doppler width is ~ 100 MHz, and few atoms are excited by the pump fields. To reduce the Doppler width, the Doppler shifts are compensated by means of two opposing magnet coils, which provide a Zeeman shift that varies linearly with position along the laser beam axis.⁷ The

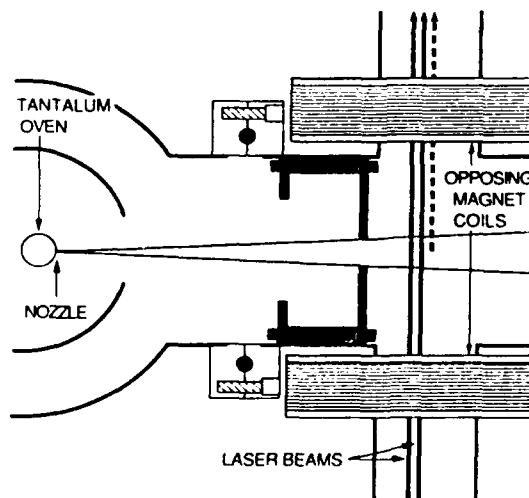


Fig. 1. Magnetically compensated beam showing the pump beams and the echo.

Zeeman shift gradient is chosen so that the $^7D_1, M = 1$ state (g factor 2.83) is resonant with the Doppler-shifted laser frequency at each position along the laser beam axis. This method is closely related to that employed previously for laser cooling, in which a spatially varying Zeeman shift compensates for the Doppler detuning that arises as the atoms are slowed.¹⁰ For optimum magnetic-field gradient, the Doppler width is reduced to 5 MHz, so that the transit time bandwidth is adequate to excite most atoms and a large echo signal is obtained. By contrast, without magnetic compensation, echo signals are reduced by more than two orders of magnitude. The signals are observed through a crossed linear polarizer so that the circularly polarized echo and the circularly polarized free-induction decay signals induced by the pump fields are of similar intensity, while the pump fields are blocked. These signals are imaged onto a Reticon diode array (spacing 25 μm). The laser is servo stabilized to the atomic resonance frequency to eliminate long-term drift. A typical echo signal is shown in Fig. 2. Note that the first $\pi/2$ pulse is more effective than the second π pulse in producing free-induction decay signals, so that the lower-intensity pulse yields the larger transmitted signal.

The presence of a magnetic-field gradient in addition to residual Doppler broadening leads to a quadratic time dependence for the phase of the macroscopic polarization in the atom frame. This alters the variation of the echo intensity with position along the atomic propagation axis from that normally expected for a two-pulse echo, as shown in Fig. 3. For narrow pump beams, the basic features of echo formation in a compensated beam can be derived by using heuristic arguments as follows. We take the atomic beam axis in the y direction, with the center of the first pump region at $y = y_1$ and that of the second pump region at $y = y_2$. For an atom of velocity v , optical polarization is created in the first interaction region at time $t_1 = y_1/v$, assuming that the atom is at the oven nozzle at $t = 0$. The polarization acquires a phase that is just the time integral of the instantaneous optical frequency. The instantaneous optical frequency differs from the natu-

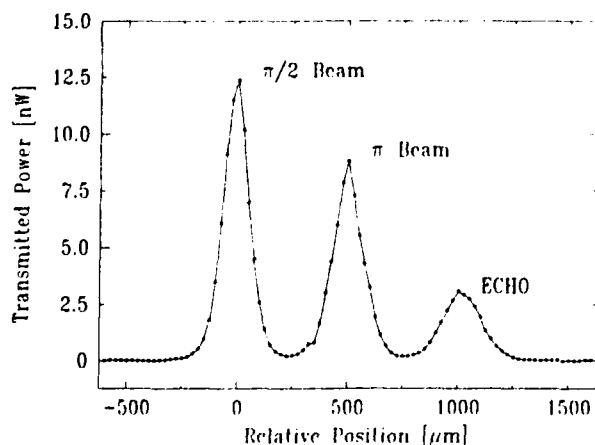


Fig. 2. Continuous spatial photon echo. The pump beams viewed through a crossed linear polarizer appear on the left. The echo signal is the rightmost peak.

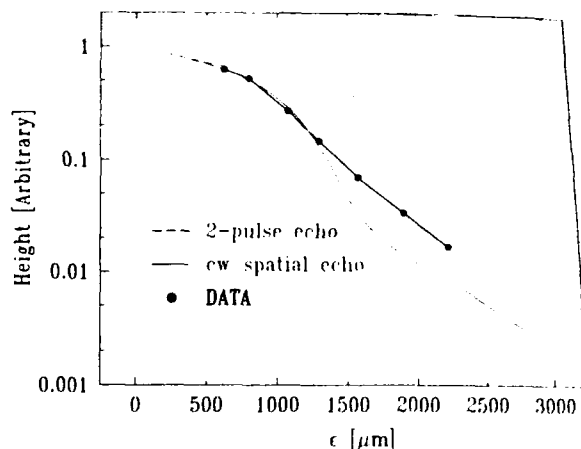


Fig. 3. Decay of the spatial echo intensity with position. The data points are obtained by translating the position of the π beam relative to the $\pi/2$ beam.

ral frequency owing to the Doppler shift kv_z and the Zeeman shift $-\alpha z$, where the z axis is taken as the laser beam axis and $k = 2\pi/\lambda$ is the optical wave vector. The Zeeman shift $-\alpha z = -(g\mu_0/\hbar)(\partial B/\partial z)z$ is assumed to vary linearly with position along the z axis. The atomic position at time t is $y = v_y t$ and $z = v_z t$. Hence, the frequency of the polarization for times $t \geq t_1$ is $\Delta(t) = kv_z - \alpha v_z t$. The net phase accumulated for an atom traveling between the two regions is then $\varphi_{21} = \int_{t_1}^{t_2} dt \Delta(t) = kv_z(t_2 - t_1) - \alpha v_z(t_2^2 - t_1^2)/2$. If we assume that in traversing the second region the atomic Bloch vector is rotated through a π angle, the accumulated phase is reversed. Following this, the atom propagates downstream to a position y , where its accumulated phase is $\varphi(y) \equiv \int_{t_1}^t dt \Delta(t) - \varphi_{21}$, with $t = y/v_y$. Hence, the phase of the optical polarization at position y is

$$\varphi(y) = k \frac{v_z}{v_y} (y - 2y_2 + y_1) - \frac{\alpha}{2} \frac{v_z}{v_y^2} (y^2 - 2y_2^2 + y_1^2). \quad (1)$$

For the supersonic beam, the velocity component v_y is distributed as a Gaussian with a narrow spread u about the mean speed v_0 . The net optical dipole moment is obtained by integrating the atomic dipole moment over the speed distribution and over the interaction volume. The path length along the laser propagation direction is proportional to the angle $\theta = v_z/v_y$. The dipole moment then is proportional to

$$\langle \exp[i\varphi(y)] \rangle = \sin \phi_1 \frac{1 - \cos \phi_2}{2} \int_{-\theta_{\max}}^{\theta_{\max}} \frac{d\theta}{2\theta_{\max}} \times \int_{-\infty}^{\infty} \frac{dv_y}{u\sqrt{\pi}} \exp\left[-\left(\frac{v_y - v_0}{u}\right)^2\right] \exp[i\varphi(y)], \quad (2)$$

where the pulse areas in the atom frame are ϕ_1 and ϕ_2 for pump regions 1 and 2, respectively. In writing Eq. (2), we assume that the residual Doppler detuning is small compared with the transit time bandwidth and the Rabi frequencies. The integral over θ is readily

carried out. For simplicity, we assume that the magnetic-field gradient is chosen for ideal frequency compensation in the first pump region at $y = y_1$, so that $\partial\varphi/\partial y = 0$ at $y = y_1$. Then $\alpha = kv_0/y_1$. Since the pump beams and echo occur within approximately a millimeter of y_1 , with $y_1 = 14$ cm, we define $y = y_1 + \epsilon$ and $y_2 = y_1 + \epsilon_2$. In this case, for $\pi/2$ and π pulses in pump regions 1 and 2, the dipole moment is then proportional to

$$\langle \exp[i\varphi(y)] \rangle = \int_{-\infty}^{\infty} \frac{M_0 dx}{\sqrt{\pi}} \exp(-M_0^2 x^2) \times \frac{\sin \left\{ q\theta_{\max} \left[(\epsilon - 2\epsilon_2) \frac{x}{x+1} - \frac{\epsilon^2 - 2\epsilon_2^2}{2y_1} \frac{1}{x+1} \right] \right\}}{q\theta_{\max} \left[(\epsilon - 2\epsilon_2) \frac{x}{x+1} - \frac{\epsilon^2 - 2\epsilon_2^2}{2y_1} \frac{1}{x+1} \right]}, \quad (3)$$

where $x = (v_x - v_0)/v_0$ and $M_0 = v_0/u$ is the Mach number. From Eq. (3), it is clear that the spread in the speed distribution leads to dephasing, and rephasing tends to occur at position $\epsilon = 2\epsilon_2$ (i.e., at twice the separation between the two pump regions). However, the quadratic dependence of the phase on distance that arises from the magnetic-field gradient favors rephasing at a point where $\epsilon^2 = 2\epsilon_2^2$. Indeed, as $u \rightarrow 0$ at high Mach numbers, $x \rightarrow 0$, and the rephasing point is $\epsilon = \sqrt{2}\epsilon_2$. For pump region separations ϵ_2 of ~ 1 mm, the quadratic position dependence of phase of the sine function dramatically alters the dependence of the echo intensity on position from the first pump region from that expected for usual two-pulse echoes. Our initial measurements of echo intensity versus pump-beam separation are in qualitative agreement with Eq. (3) assuming a Mach number $M_0 = 5$, after averaging over a spread of ϵ_2 in order to account for the finite pump-beam diameter as shown in Fig. 3. However, complete quantitative agreement has not yet been obtained.

In conclusion, we have demonstrated a method for preparing and transporting a large macroscopic optical coherence over millimeter distances, so that optical coherence can be observed in a region free of all pump fields. While the local frequency compensation technique demonstrated in Ref. 7 can be used to obtain large signals, the observed decay of the echo intensity with increasing distance shows that the quadratic time dependence of the optical phase (for the present magnetic-field gradient configuration) limits the maximum distances over which coherence can be transported without dephasing.

The method demonstrated in this Letter is ideally suited to developing spatial field convolution and correlation techniques. Such techniques have been explored previously using four-wave mixing,¹¹ except that the individual interactions with the input fields were not spatially separated. As applied to optical processing, our techniques are the spatial analogs of the methods used in the time domain based on stimulated echoes.^{2,12} The present experiments achieve a spatial resolution of $25 \mu\text{m}$ limited by the Reticon diode array. Much higher spatial resolution (up to the diffraction limit) is attainable by magnification of the echo image and increasing the bandwidth of the medium, which is fully adjustable. In addition, optical Bloch vector noise can be studied as a function of the Bloch angle¹³ by using a cw pump fields and measuring the phase-dependent noise in the cw echo signals. Finally, the method is well suited to study the evolution of optical coherence in cavities¹⁴ in which the emitted field can be measured directly and continuously by optical methods.

This research is supported by the Rome Air Development Center under contract F19628-88-K-0012.

References

1. N. A. Kurnit, I. D. Abella, and S. R. Hartmann, *Phys. Rev. Lett.* **13**, 567 (1964).
2. Y. S. Bai, W. R. Babbitt, N. W. Carlson, and T. W. Mossberg, *Appl. Phys. Lett.* **45**, 714 (1984).
3. See T. W. Mossberg, *Opt. Lett.* **7**, 77 (1982).
4. A. Rebane, R. Kaarli, P. Saari, A. Anijalg, and K. Timpmann, *Opt. Commun.* **47**, 173 (1983).
5. A. Rebane, J. Aaviksoo, and J. Kuhl, *Appl. Phys. Lett.* **54**, 93 (1989).
6. See, for example, J. C. Bergquist, S. A. Lee, and J. L. Hall, *Phys. Rev. Lett.* **38**, 159 (1977).
7. K. D. Stokes, C. Schnurr, J. Gardner, M. Marable, S. Shaw, M. Goforth, D. E. Holmgren, and J. E. Thomas, *Opt. Lett.* **14**, 1324 (1989).
8. Photon echoes can be considered as limited superradiance. See M. S. Feld, in *Frontiers in Laser Spectroscopy*, R. Balian, S. Haroche, and S. Liberman, eds. (North-Holland, New York, 1977).
9. S. N. Bagayev, V. P. Chebotayev, and A. S. Dychkov, *Appl. Phys.* **15**, 209 (1978).
10. See, for example, W. D. Phillips, J. V. Prodan, and H. J. Metcalf, *J. Opt. Soc. Am. B* **2**, 1751 (1985).
11. J. O. White and A. Yariv, *Appl. Phys. Lett.* **1**, 37 (1980).
12. See M. K. Kim and R. Kachru, *Opt. Lett.* **14**, 423 (1989), and references therein.
13. B. Vodiemicz and J. H. Eberly, *J. Opt. Soc. Am. B* **2**, 458 (1985); P. K. Aravind, *J. Opt. Soc. Am. B* **3**, 1712 (1986).
14. J. Krause, M. O. Scully, and H. Walther, *Phys. Rev. A* **34**, 2032 (1986).

Uncertainty-limited position measurement of moving atoms using optical fields

J. E. Thomas

Department of Physics, Duke University, Durham, North Carolina 27706

Received May 11, 1989; accepted August 1, 1989

A method for measuring atomic spatial distributions is suggested, based on Raman transitions in an applied force field. This technique eliminates the Doppler effect and provides high-frequency resolution for long-lived states, leading to position resolution that is fundamentally limited by the uncertainty principle. The effects of atomic motion are discussed, and a simplified analysis of the method is presented.

Recently there has been substantial progress and interest in the creation of atomic distributions that vary over small length scales by diffraction,¹ periodic spatial modulation,² channeling,³ focusing,⁴ and cooling.⁵ In general, such distributions exhibit momentum-space coherence and are of both practical and fundamental interest. These developments have been carried on, in part, by the advent of practical laser cooling techniques.⁶ Important applications include atomic interferometry and the creation of submicrometer structures by atomic deposition.^{1,2} While techniques exist to create suboptical-wavelength atomic spatial modulation and interference, with the exception of the technique described in Ref. 3, which is described below, methods for detection have been limited principally to hot wires, so far as the author is aware.

In this Letter a class of techniques is suggested that may prove useful in achieving much higher spatial resolution of moving atoms by using optical fields and that examine interesting features of quantum-mechanical position measurement.

The method for making the measurements is in principle quite simple. Suppose that an atom in a state (0; Fig. 1) enters a region of potential that, for simplicity, varies linearly in one spatial direction x and affects only level 2. Then the potential can be written as

$$V(x) = -(x - x_0)F, \quad (1)$$

where F is a constant force. A number of techniques can be used to generate such a potential, some of which are described below. The basic idea is to use the fact that for a transition from level 0 to 2, the spatially varying potential correlates the resonance frequency of the atom with its position, so that optical fields of sufficient frequency resolution can select out atoms at one particular position, analogous to a nuclear magnetic resonance imaging technique. Doppler frequency shifts, which broaden the line for one-photon transitions, are readily eliminated by using a copropagating wave Raman-induced optical resonance⁷ (Fig. 1) or any other Doppler-free coherent process connecting long-lived states. In the Raman transition, it is the

difference between the frequencies of two optical fields that must resonate with the atomic system, and the Doppler shift approximately cancels, so the position measurement can be made independent of velocity. The above potential shifts the final atomic state 2 and tunes the Raman resonance frequency to make it spatially dependent with a frequency gradient $F/\hbar = d\omega/dx$. In practice, the optical field difference frequency can be taken as the unperturbed initial-to-final spacing, so that the above potential selects out atoms at position $x = x_0$, the position at which the net frequency shift of the spatially varying potential is zero. This position is readily moved by varying, for example, a small uniform magnetic field, which is superimposed upon the spatially varying potential.

An important feature of the Raman technique is that it corresponds to the absorption of a photon from one optical field and the emission of a photon into another, copropagating, field. Hence the net momentum imparted by the Raman optical fields to the atom is approximately zero, since the difference frequencies of interest here are small. This has the interesting consequence that the accuracy of the measurement is fundamentally limited by the Heisenberg uncertainty principle, even when the Raman fields propagate along the measurement axis. Before we discuss other limiting factors that are due to the atomic motion, it is useful to consider this limit. First, consider the frequency resolution required to obtain a spatial resolu-

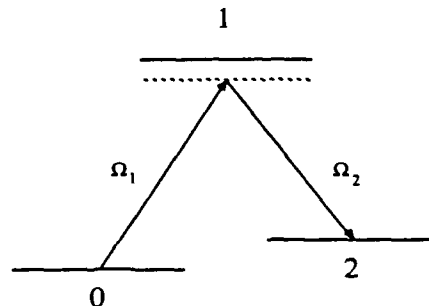


Fig. 1. Three-level system and Raman fields. Atoms initially are in state 0.

tion Δx . The resonance frequency shift across the spatial resolution length scale must equal the frequency resolution:

$$F\Delta x/\hbar = 1/T. \quad (2)$$

Since the initial and final atomic states are taken as long-lived excited states or ground states, the frequency resolution will be limited by the interaction time T of the atom with the optical field. Hence $\Delta x = \hbar/(FT)$. Raman transitions can occur at any time in the Raman region, so the maximum momentum imparted by the potential is just $p_{\max} = FT$. Estimating $\Delta p \sim p_{\max}$ yields $\Delta x \Delta p = \hbar$, which determines the fundamental limit. Thus the resolution accuracy is determined by the spatially varying potential according to the uncertainty principle, and no excess momentum is imparted by the measurement light field.

As described below, a number of techniques are available for producing spatially varying level shifts of 10^{10} Hz/cm over millimeter distances, with much larger shift gradients obtainable for smaller maximum distances. Assuming a transit-time limited resolution of 100 kHz, the corresponding spatial resolution is 0.1 μm . By using a Raman-induced optical resonance technique, it is easy to obtain much better frequency resolution than 100 kHz by increasing T . However, as T increases, the atomic motion limits the spatial resolution. In the simplest case, the spatial resolution will be limited by the velocity of the atoms along the measurement axis. To determine the natural scale of resolution, we equate the interaction time T with the transit time of the atoms across the resolution length. If we take the atomic beam to be principally propagating along the y axis with velocity v_y and with a component of velocity along the measurement x axis, v_x , then the time to cross the resolution length is $T = \Delta x/v_x$. The corresponding frequency resolution is $1/T = v_x/\Delta x$. Using this in Eq. (2) and solving for Δx yields

$$\Delta x_{\text{VEL}} = (\hbar v_x/F)^{1/2}. \quad (3)$$

A frequency gradient of 10^{10} Hz/cm gives $\Delta x_{\text{VEL}} = 0.04 \mu\text{m} [v_x (\text{cm/sec})]^{1/2}$. For a supersonic beam of velocity $v_y = 10^5$ cm/sec, modest collimation of 1 mrad would yield $c_x = 100$ cm/sec and a spatial resolution of $\sim 0.4 \mu\text{m}$. The optical laser beam width d must then be chosen for consistency such that the laser beam transit time equals the transit time across the spatial resolution length: $d = \Delta x(v_y/v_x) = 0.4 \mu\text{m}/(1 \text{ mrad}) = 0.4 \text{ mm}$. In this way, the longest transit time possible is used, for which the atom does not travel any farther across the frequency gradient than the resolution length. For this reason, optical lasers are particularly well suited to limiting the interaction time by focusing.

If the velocity along the measurement axis is sufficiently small, the acceleration due to the spatially varying potential is a limiting factor. In this case, equating the resolution length with the position change due to the acceleration yields the maximum interaction time T . Inserting this into Eq. (2) yields the optimum resolution as

$$\Delta x_{\text{ACCEL}} = (\hbar^2/2MF)^{1/3}. \quad (4)$$

For consistency, the laser beam width is chosen as $d =$

$v_y T$ to limit the interaction time. In this case, the momentum imparted by the force limits the measurement accuracy, so this limit is in some sense the uncertainty limit. For a sodium atom, a 10^{10} -Hz/cm frequency gradient yields a resolution of 0.06 μm . For a velocity perpendicular to the laser of 10^5 cm/sec, the corresponding laser beam width is 2.5 mm. The condition for the velocity along the measurement axis to dominate the resolution is for $\Delta x_{\text{VEL}} \geq \Delta x_{\text{ACCEL}}$. This requires that the velocity v_x be such that $v_x \geq \Delta x_{\text{ACCEL}}^2 F/\hbar$, which is equivalent to $v_x \geq \hbar/(2M\Delta x_{\text{ACCEL}})$. For the above conditions this yields $v_x \geq 2$ cm/sec.

Omitted in the above discussion are the limits imposed by the atomic distribution itself. In general, any atomic beam will have some finite transverse velocity spread. In a state possessing momentum-space coherence, the different kinetic energies corresponding to different momentum components will cause periodic spatial modulation to wash out when the (incoherent) transverse velocity averaging is performed. This problem has been solved by having the atoms traverse multiple separated laser fields to initiate rephasing.² If the atomic pattern varies more slowly than Δx_{VEL} , the rephasing length will be longer than the laser beam width. A more fundamental limit is due to wave-packet spreading. In this case, an atomic distribution that varies over a length a will spread a distance of order a over a time T_{MAX} such that $(\hbar/2Ma^2) T_{\text{MAX}} \sim 1$. The transit time across the resolution length must be limited to T_{MAX} . Using this in Eq. (2) leads to a resolution limit of $\Delta x_{\text{SPREAD}} = (\Delta x_{\text{ACCEL}})^3/a^2$. Hence, as long as the scale of spatial variation is larger than Δx_{ACCEL} , wave-packet spreading during the measurement poses no problem.

Spatially varying frequency shifts can be produced by a variety of methods, the most obvious of which is the use of Stark or Zeeman shifts. The latter have been explored extensively for atomic beam deflection applications.⁸ Field gradients larger than 10^4 G/cm are obtained by using hollow water-cooled two-wire configurations and millimeter wire spacings, with atoms propagating parallel to the wires. In order to obtain a level shift that varies along one direction without violating the divergence or curl conditions, a uniform bias field is applied, either as part of the two-wire field or as an additional field. The effect of this uniform field is to suppress the component of the spatially varying field perpendicular to the bias field so that its effect on the level shift is of second order in distance. For sufficiently large bias fields, the level shift due to the unwanted field variation over the largest distances measured can be made smaller than the linear variation in the level shift over the resolution length.

An interesting alternative for obtaining spatially varying level shifts is to exploit the light shift as shown in Fig. 2. This has been demonstrated for the case of atoms channeled in a nonresonant standing wave. Spatial variation of the light shift due to the trapping light field was used to deduce the periodic variation of atomic density from the one-photon absorption spectra.³ For position measurement (Fig. 2), two nonresonant linearly polarized laser beams of wave vector q ,

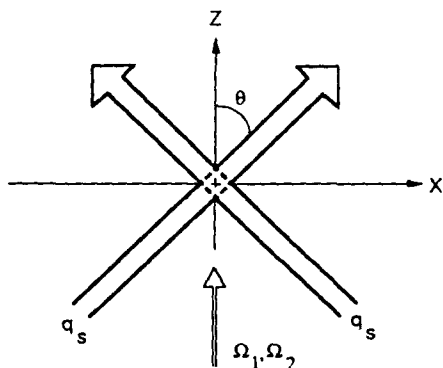


Fig. 2. Spatial-frequency gradient based on the light shift of two overlapping laser beams. Atoms propagate into the page along the y axis. Ω_1 and Ω_2 are the Raman laser fields.

intersect at an angle 2θ and are used to shift the final state 2. The light shift, which is proportional to the intensity in lowest order, has a spatial variation $\propto 1 + \cos(2q_s x \sin \theta)$. Physically, a force results from interactions in which an off-resonant state (state 2 in this case) absorbs momentum from one beam and emits into the other, so that the net momentum transferred to the atom during the interaction time T is just FT , as in the above discussion. By adjusting the intersection angle, the length scale over which the light shift varies can be conveniently controlled. For reasonable detunings and laser powers, very large frequency gradients are obtainable over small maximum spatial dimensions. For example, a maximum light shift of only 10 MHz over 10- μ m distances would yield frequency gradients of 10^{10} Hz/cm. For measurement of periodic spatial patterns that vary at multiples of the optical wave vector, a standing-wave light shift can be used to obtain gradients of 10^{12} Hz/cm at moderate laser intensity. The resonance position x_0 can be varied near the maximum derivative point either by means of a superposed uniform Zeeman field or by tuning the Raman laser field difference frequency. Finally, the system can be calibrated by using atomic distributions of known periodic spatial variation produced by any convenient method,¹⁻³ and the shifting fields can be stabilized by using an atomic resonance. It is expected that, for long-lived atomic states, high spatial resolution can be obtained in this way, provided that the interaction time is limited to the optimum value, as discussed above.

Detailed calculations that support the simple arguments discussed above have been carried out for the level scheme of Fig. 1, treating the center-of-mass mo-

tion for the atom quantum mechanically and including a constant force that acts on level 2 only.⁹ An important feature is that the detection system for the final state need not have any spatial resolution. In general, any convenient means for final-state detection, including fluorescence, photon burst, and photoionization, is applicable. This permits single-atom detection schemes and either ground states or reasonably long-lived excited states to be employed for the measurements.

The maximum state 2 count rate is given by the product of the Raman transition probability, η_R , the detection efficiency, η_D , the flux in state 0, $n\nu_y$, and the effective interaction area that is the product of the atomic beam width perpendicular to the measurement axis, l_z , and the spatial resolution, Δx_{OPT} . For $n = 10^9/\text{cm}^3$ and $\nu_y = 10^5$, $l_z = 0.1$ mm, $\Delta x_{OPT} = 0.1$ μ m, the count rate is $\eta_D \eta_R / 10^7/\text{sec}$. Taking $\eta_R = 0.1$ and $\eta_D = 0.1$ yields a count rate of $10^5/\text{sec}$.

Particularly interesting atomic systems for measurements are the $^7F_1 \rightarrow ^7F_0$ transition in ^{154}Sm and the $^1S_0 \rightarrow ^3P_1$ transitions of ^{174}Yb and ^{88}Sr . The latter two have a long radiative lifetime and a $J = 0$ ground state with no nuclear spin. They can be used by exploiting the excited-state splittings and should be important for atomic interference experiments for which unwanted level shifts before the detection region would pose a problem.

The author is indebted to D. Holmgren and J. Gardner for many stimulating conversations about this work. This research is supported by Rome Air Development Center contract F19628-88-K-0012.

References

1. See P. E. Martin, B. G. Oldaker, A. H. Miklich, and D. E. Pritchard, *Phys. Rev. Lett.* **60**, 515 (1988), and references therein.
2. V. P. Chebotayev, B. Ya. Dubetsky, A. P. Kasantsev, and V. P. Yakovlev, *J. Opt. Soc. Am. B* **2**, 1791 (1984).
3. C. Salomon, J. Dalibard, A. Aspect, H. Metcalf, and C. Cohen-Tannoudji, *Phys. Rev. Lett.* **59**, 1659 (1987).
4. V. I. Balykin and V. S. Letokhov, *Phys. Today* **42**(4), 23 (1989).
5. A. Aspect, E. Arimondo, R. Kaiser, N. Vansteenkiste, and C. Cohen-Tannoudji, *Phys. Rev. Lett.* **61**, 826 (1988).
6. See, for example, W. D. Phillips, J. V. Prodan, and H. J. Metcalf, *J. Opt. Soc. Am. B* **2**, 1751 (1985).
7. J. E. Thomas, P. R. Hemmer, S. Ezekiel, C. C. Leiby, Jr., R. H. Picard, and C. R. Willis, *Phys. Rev. Lett.* **48**, 867 (1982).
8. N. F. Ramsey, *Molecular Beams* (Oxford U. Press, London, 1956).
9. J. E. Thomas, K. D. Stokes, J. Gardner, and C. Schnurr, "Ultrahigh-resolution position measurements using optical fields," to be submitted to *Phys. Rev. A*.

Quantum theory of atomic position measurement using optical fields

J. E. Thomas

Department of Physics, Duke University, Durham, North Carolina 27706

(Received 23 February 1990; revised manuscript received 11 June 1990)

A simple quantum theory of recently suggested optical techniques for ultrahigh-resolution position measurement and localization of moving atoms in beams is presented. Both the internal and center-of-mass motion are treated quantum mechanically so that the limitations on the ultimate position resolution due to atomic motion and wave-mechanical diffraction are included in the analysis. The techniques utilize a miniaturized form of Raman-induced resonance imaging in which optical fields are used to make transitions from a long-lived initial state to a long-lived final state. The final state is shifted by the spatially varying potential of an applied force field in order to correlate the atomic position with its resonance frequency. Spatially varying level shifts are obtainable by using very large Zeeman field gradients or spatially varying light shifts in a small interaction volume. This results in very high spatial resolution. The atomic transit time across the optical-field region is limited by focusing to an ideal diameter that minimizes the spatial resolution length. The results of the analysis show that nanometer spatial resolution of the initial-state position distribution is attainable. Under appropriate conditions, the final-state spatial wave function can take the form of a minimum-uncertainty Gaussian wave packet obeying $\Delta x \Delta p = \hbar/2$. Such states may prove useful in studying one-dimensional wave-packet motion in applied potentials.

I. INTRODUCTION

Recently there has been substantial progress and interest in the creation of atomic distributions which vary over small length scales. In atomic beams, such distributions arise by diffraction,¹ periodic spatial modulation,² channeling,³ focusing,⁴ and cooling.⁵ In general, the distributions exhibit momentum-space coherence and are of both practical and fundamental interest. These developments have been spurred on, in part, by the advent of practical laser-cooling techniques.⁶ Important applications include atomic interferometry, gyroscopes, and the creation of submicrometer structures by atomic deposition.^{1,2}

While techniques exist to create suboptical-wavelength atomic spatial modulation and interference in atomic beams, methods for detection have been limited principally to hot wires. Only in Ref. 3 is optical absorption used to determine the atomic position distribution. In that work, atoms are channeled in an off-resonant optical standing wave. Due to the spatial variation of the light shifts in the standing wave, atoms at a node resonate at a different frequency than atoms at a peak in the optical field. Thus, a two-peak absorption spectrum is obtained in which the height and shape of the peaks vary when the atoms are redistributed by channeling, compared to when they are not channeled. Since the channeling field and the spatially varying light shift which causes the channeling vary with the same scale of length, the true periodic structure of the channeled atomic distribution could not be directly measured in the experiments. While the position resolution obtained was adequate (although not specified in Ref. 3), it was limited by the spontaneous linewidth for the transition employed as well as by Doppler broadening. Further, the diameter of the interaction region (4.6 mm) was chosen to achieve channel-

ing without heating. In this case, the interaction time is long enough for the atoms to be redistributed over distances comparable to an optical wavelength. For optimum position resolution, our calculations show that the interaction time of the atoms with the measurement field must be much shorter, since the atoms must move no more than the optimum resolution length. This is much shorter than an optical wavelength for the large light shifts employed in the experiments.

The purpose of this paper is to analyze a recently suggested class of techniques⁷ which may prove useful in achieving much higher spatial resolution of moving atoms using optical fields than has been obtained previously. We begin by reviewing the principal features of the method using heuristic arguments and then proceed to the detailed derivation.

The basic method, Fig. 1, is to use a spatially varying potential $V(x)$, which makes the resonance frequency of simple atoms position dependent, analogous to magnetic resonance (MR) imaging. Unlike conventional MR imaging, the proposed method employs Raman-induced resonance imaging using optical fields. The use of optical fields permits the measurements to be made in very small volumes with very large spatially varying potentials, which leads to quantum-mechanical limits on the ultimate measurement accuracy. As shown in Fig. 1, the atoms enter the Raman interaction region in a long-lived initial state (i) which is *not* shifted by the potential $V(x)$ and make a transition via two optical fields to a long-lived final state (f) which is shifted by the applied potential. In this way, the atomic position and its resonance frequency are correlated. The total number of atoms emerging in the final state is measured downstream from the Raman region. This signal is proportional to the number of atoms in the initial state which make a transition to the final state near the position where the optical fields

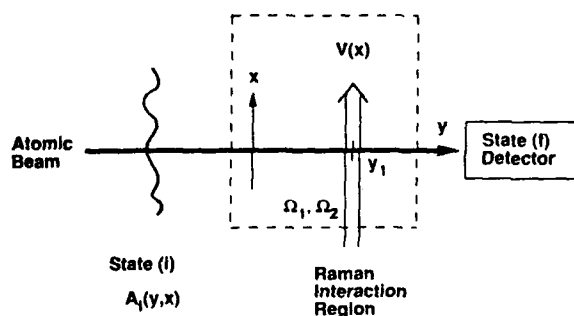


FIG. 1. Atomic-position measurement by Raman-induced resonance imaging. Atoms enter the Raman interaction region in an initial state i with some spatial distribution along the measurement axis x which is to be measured. The initial-state amplitude $A_i(y, x)$ is presumed to be specified at the plane $y = y_1$ centered in the Raman fields Ω_1, Ω_2 . A spatially varying potential $V(x)$ shifts the final state f without affecting the initial state i and correlates the Raman resonance frequency with the atomic position along the x axis. Atoms which are detected downstream in state f are those which have made the $i \rightarrow f$ transition in a narrow spatial region Δx where the Raman fields are resonant for the $i \rightarrow f$ transition.

are resonant with the Raman transition. The goal is to measure prepared *incident* atomic distributions without modification due to trapping or channeling, by appropriately limiting the interaction time. These techniques examine interesting features of quantum-mechanical position measurement and should make it possible to localize atoms to much better than an optical wavelength for application to a variety of interesting experiments. For the ^{154}Sm or ^{174}Yb systems we are currently studying, it should be possible to achieve position resolution of ≈ 70 Å.

An important feature of the analysis is that it determines the ultimate spatial resolution attainable for *moving* atoms in large spatially varying level shift gradients which correlate the atomic resonance frequency with position. The results should have important bearing on experiments which measure the interaction of atoms with surfaces.⁸

Finally, it is shown below that the center-of-mass wave function for atoms which emerge in the final state is highly localized and, under appropriate conditions, can take the form of a minimum uncertainty Gaussian wave packet. These results complement recent work on atomic and molecular internal state wave packets.⁹

For optimum position resolution, it is necessary that both radiative and Doppler broadening, as well as the laser linewidth, be negligible compared to transit-time broadening. In some cases, a one-photon transition from the ground state is adequate. This would require a long-lived excited state, large spatially varying level shifts, and high atomic-beam collimation. Alternatively, a Raman-induced resonance between long-lived ground states can be used,⁷ as mentioned above and described below.

To explain the Raman-induced resonance imaging method in more detail, suppose that an atomic beam is prepared in an initial long-lived internal state (i) with

some interesting spatial distribution perpendicular to the atomic-beam propagation axis. To measure the spatial distribution, the atoms enter an interaction region containing two optical fields of frequencies Ω_1, Ω_2 which can induce Raman transitions between the long-lived initial state and a long-lived final state f . The interaction region also contains a spatially varying potential which makes the Raman resonance frequency dependent on the spatial position of the atom. For simplicity, suppose that the spatially varying potential is due to a uniform force F which affects only the final state (f) of the atom. The potential is taken to vary linearly along the x axis, which is perpendicular to the atomic-beam propagation direction, and which ultimately will become the measurement axis. For concreteness, let $x_0 F$ be the shift of the final state due to a uniform Zeeman field, and $-x F$ be the shift of the final state due to an additional Zeeman shift or light shift which varies linearly in space. The net potential can be written as

$$V(x - x_0) = -(x - x_0)F. \quad (1)$$

Further, suppose that the atoms which enter this potential in the internal state (i) are *not* shifted. In this case, the $i \rightarrow f$ resonance frequency varies linearly in space, so that a resonance field of sufficient frequency resolution can cause $i \rightarrow f$ transitions in a highly localized region Δx along the x axis. The position resolution Δx is determined by the potential-energy change $\Delta V = F\Delta x$ and the frequency resolution $\Delta\omega$ according to

$$\frac{F}{\hbar} \Delta x = \Delta\omega \equiv \frac{1}{T^*}, \quad (2)$$

where T^* is the effective interaction time which determines the frequency resolution. If a one-photon optically allowed transition is employed, then the frequency resolution will be limited by Doppler and radiative broadening as well as by laser-frequency jitter. All of these deficiencies are remedied by using a copropagating-wave Raman-induced resonance between long-lived states (i) and (f) via some off-resonant intermediate state (I) as shown in Fig. 2.

The optical fields Ω_1, Ω_2 are taken to copropagate. By choice of the difference frequency $\Omega_2 - \Omega_1$, a Raman resonance with the $i \rightarrow f$ transition frequency ω_{fi} can be made to occur at the point $x = x_0$ along the measurement axis. The Raman fields are derived by A/O modulation from the laser field ω so that the difference frequency is easily made very stable. By using an off-resonant Raman transition and copropagating fields, the laser jitter, beam divergence, Doppler shifts, etc., drop out, since only the difference frequency enters. This technique was employed previously to obtain Raman-induced Ramsey resonances using optical fields, where 100-Hz resolution was readily obtained.¹⁰ By monitoring the total count rate of atoms in state f emerging from the Raman region versus uniform Zeeman shift (which varies x_0), the incident spatial distribution in state i is determined. Only initial state atoms near $x = x_0$, the point at which $\Omega_1 - \Omega_2 = \omega_{fi}$, contribute to the signal.

The use of optical fields in the measurement leads to a

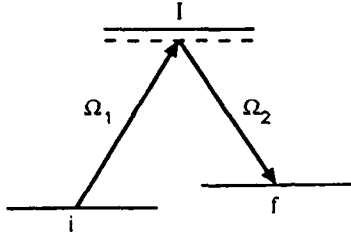


FIG. 2. Level scheme and Raman fields.

number of new features which are listed briefly here.

(1) *Spatially Varying Level Shifts.* Two-wire magnetic-field gradients as developed for atom-deflection applications can be used to achieve spatially varying level shifts $F/\hbar = 10^{10}$ Hz/cm over millimeter length scales. Over smaller maximum distances, very large spatially varying level shifts can be obtained by using the light shifts of intense, nonresonant intersecting laser beams (*not* the Raman beams). In this case, more than 10^{12} Hz/cm is feasible. Spatially varying shifts this large have been used in atom-channeling experiments, but application to position measurements which yield the incident spatial distribution have not been explored. When the interaction time is optimally limited as described below, exceedingly high spatial resolution is attainable.

(2) *Spatial Resolution.* When long-lived states (i, f) are chosen for measurement, the interaction time T^* is determined by the atom transit time T across the Raman region. In this case, the use of optical fields allows the interaction time to be limited to an optimum value by focusing. The optimum value of T is determined by the criterion that the atom not move across the ideal resolution length during the measurement. The simplest limit is due to the atomic velocity component v_x along the measurement axis. In this case, the optimum interaction time is $T = \Delta x / v_x$. With Eq. (2), the optimum spatial resolution is given by

$$\Delta x_{\text{vel}} = \sqrt{\hbar v_x / F} \quad (3)$$

For modest atomic-beam collimation and a two-wire magnetic-field gradient, *suboptical-wavelength* position resolution is readily attainable.

For a highly collimated atomic beam, v_x no longer limits the interaction time. In this case, the acceleration due to the applied force and diffraction out of the resolution length limit the smallest regions which are measurable. For the acceleration limit, the optimum value of the interaction time is such that $(F/2M)T^2 = \Delta x$. For the diffraction limit, the interaction time must be such that a particle localized into a region of length Δx spread only over distances comparable to Δx , i.e., $(\hbar/2M\Delta x)T = \Delta x$. In either case, with Eq. (2), the optimum resolution is

$$\Delta x_{\text{accel}} = \left[\frac{\hbar^2}{2MF} \right]^{1/3}, \quad (4)$$

which we will refer to as the acceleration limit. To achieve this limit, we must have $v_x < \hbar/(2M\Delta x_{\text{accel}})$, as shown below. For a 10^{12} -Hz/cm light-shift gradient, the

optimum resolution is about 70 Å for samarium and the required collimation for a beam of speed 6×10^4 cm/s is $50 \mu\text{rad}$, which is not too stringent.

(3) *Uncertainty limit.* Since the force due to the spatially varying potential acts on the atom only after it makes a transition from the initial unshifted state, the momentum uncertainty imparted by the force, Δp , is approximately equal to the maximum momentum imparted, FT . Using Eq. (2) we see that the final state is created with a spatial resolution and momentum spread which obey the uncertainty relation $\Delta x \Delta p \approx \hbar$. In Sec. III B it is shown that *minimum* uncertainty packets can be created under appropriate conditions.

(4) *Detection.* The method for detecting the final state (f) need not have any spatial resolution since the measurement is done by the Raman region. Only the spatial integral of the final-state flux is needed, therefore a variety of final-state detection schemes are possible. These include resonance fluorescence, and single-atom methods such as photon burst and photoionization, which have been successfully applied to trace-element measurement.

II. THEORY

In the following, we consider the Raman-induced resonance imaging scheme⁷ in detail. Schemes based on one-photon transitions, when appropriate, yield analogous results and need not be derived in depth. A three-level atom with states i, I, f , as shown in Fig. 2, enters a region with a spatially varying potential which exerts a force on the state f only. The atom enters the region in state i which does *not* interact with the spatially varying potential and makes a Raman transition via two off-resonant light fields to the final state. The transition occurs in a localized region determined by the resonance condition that the initial-to-final-state frequency ω_{fi} equal the difference frequency of the two applied optical fields. The total (spatially integrated) final-state flux emerging from the Raman region is monitored downstream as a function of the Raman-field difference frequency or as a function of ω_{fi} which can be tuned by means of an applied uniform magnetic field.

In this section, the integrated flux of atoms in state f exiting the Raman region is calculated at distances large compared to the diameter of the Raman regions which are assumed to be Gaussian. The steady-state amplitude for the final state is calculated first, where it is assumed that the wave-mechanical motion is important for the x motion. An eikonal approximation is assumed to be adequate for the y coordinate along the atomic-beam axis. The Raman transition frequency ω_{fi} is taken to be very small, so that the difference in the wave vectors of the optical fields can be taken as zero. In this case, the net recoil momentum of the atom in making the Raman transition is negligible. Finally, the optical fields are assumed to be far enough off resonance with the excited state that the excited-state amplitude can be adiabatically eliminated from the coupled amplitude equations which are derived below.

The Hamiltonian for the three-level system of Fig. 2 is

taken as

$$H = \frac{\mathbf{P}^2}{2M} + H^{(0)} - \boldsymbol{\mu} \cdot \mathbf{E}(\mathbf{R}, t) - (x - x_0)F^{\text{op}}, \quad (5)$$

where $H^{(0)}$ is the internal Hamiltonian, \mathbf{P} is the atomic center-of-mass momentum operator, F^{op} is the external force operator, and x is the position along the measurement axis. The electric dipole operator is $\boldsymbol{\mu}$ and the applied field is of the form

$$\mathbf{E}(\mathbf{R}, t) = \left\{ \frac{\hat{\mathbf{e}}_1 \mathcal{E}_1}{2} e^{i(\mathbf{q} \cdot \mathbf{R} - \Omega_1 t)} + \text{c.c.} + \frac{\hat{\mathbf{e}}_2 \mathcal{E}_2}{2} e^{i(\mathbf{q} \cdot \mathbf{R} - \Omega_2 t)} + \text{c.c.} \right\} e^{-1/2[(y - y_1)/d]^2}, \quad (6)$$

where the Raman fields are assumed to copropagate and the difference frequency $\Omega_1 - \Omega_2$ is assumed sufficiently small that the wave vectors are taken to be of equal magnitude. The polarizations $\hat{\mathbf{e}}_{1,2}$ are chosen so that each field interacts with only one transition. The Raman-field region is taken to be centered at a position y_1 along the atomic-beam axis and the laser $1/e$ intensity radius along the y axis is d . Variation in the fields along directions perpendicular to the atomic-beam axis is assumed negligible. The atomic wave function is taken to be of the form

$$|\Psi(\mathbf{R}, t)\rangle = \sum_n \frac{e^{i\mathbf{k} \cdot \mathbf{R}}}{\sqrt{V}} e^{-i(\hbar \mathbf{k}^2/2M)t} A_n(\mathbf{R}, t) e^{-i\omega_n t} |n\rangle, \quad (7)$$

where the velocity of the particular atom being considered is $\mathbf{v} = \hbar \mathbf{k}/M$ prior to interaction and it is assumed that an initial velocity average will be performed at the end of the calculation. The internal state of energy $\hbar \omega_n$ is $|n\rangle$. With these assumptions, the time-dependent Schrödinger equation yields equations of motion for the state amplitudes A_n given by

$$i\hbar \left[\frac{\partial}{\partial t} + \mathbf{v} \cdot \nabla \right] A_n + \frac{\hbar^2}{2M} \nabla^2 A_n + (x - x_0) F_n A_n = - \sum_m \boldsymbol{\mu}_{nm} \cdot \mathbf{E}(\mathbf{R}, t) e^{i\omega_{nm} t} A_m, \quad (8)$$

where the force $F_n = F \delta_{nf}$ acts only on the final state. We take the Raman difference frequency equal to the $i \rightarrow f$ frequency in the absence of the force: $\Omega_1 - \Omega_2 = \omega_{fi}$. Then we seek solutions for which the initial- and final-state amplitudes are time independent but vary in space. It is assumed that the velocity perpendicular to the laser beams v_y is large (i.e., a thermal speed), while the velocity v_x along the measurement axis x is small. In this case, it is convenient to make an eikonal approximation for the y motion, retaining only the first spatial derivative term, while for the x direction, both the first and second x derivatives are retained to take into account packet spreading. Equation (8) is then easily solved in perturbation theory by finding the Green's function for states i

and f and treating the right-hand side as a source.

To proceed, Eq. (8) is rewritten explicitly using the rotating-wave approximation and takes the form

$$\begin{aligned} & \left[\frac{\partial}{\partial t} + \mathbf{v} \cdot \nabla - \frac{i\hbar}{2M} \frac{\partial^2}{\partial x^2} \right] A_i(\mathbf{R}, t) \\ &= - \frac{\Omega_{fi}^*(\mathbf{R})}{2i} e^{-i\mathbf{q} \cdot \mathbf{R} - i(\omega_{fi} - \Omega_1)t} A_f(\mathbf{R}, t), \\ & \left[\frac{\partial}{\partial t} + \mathbf{v} \cdot \nabla - \frac{i\hbar}{2M} \frac{\partial^2}{\partial x^2} - \frac{i}{\hbar} (x - x_0) F \right] A_f(\mathbf{R}, t) \\ &= - \frac{\Omega_{if}^*(\mathbf{R})}{2i} e^{-i\mathbf{q} \cdot \mathbf{R} - i(\omega_{if} - \Omega_2)t} A_i(\mathbf{R}, t), \quad (9) \\ & \left[\frac{\partial}{\partial t} + \mathbf{v} \cdot \nabla - \frac{i\hbar}{2M} \frac{\partial^2}{\partial x^2} \right] A_i(\mathbf{R}, t) \\ &= - \frac{\Omega_{fi}(\mathbf{R})}{2i} e^{+i\mathbf{q} \cdot \mathbf{R} + i(\omega_{fi} - \Omega_1)t} A_i(\mathbf{R}, t) \\ & \quad - \frac{\Omega_{if}(\mathbf{R})}{2i} e^{+i\mathbf{q} \cdot \mathbf{R} + i(\omega_{if} - \Omega_2)t} A_f(\mathbf{R}, t) \\ & \quad - \frac{\gamma_i}{2} A_i(\mathbf{R}, t), \end{aligned}$$

where $\Omega_{fi}(\mathbf{R}) = \boldsymbol{\mu}_{fi} \cdot \hat{\mathbf{e}}_1 \mathcal{E}_1(\mathbf{R})/\hbar$ and $\Omega_{if}(\mathbf{R}) = \boldsymbol{\mu}_{if} \cdot \hat{\mathbf{e}}_2 \mathcal{E}_2(\mathbf{R})/\hbar$ and the spatial dependence of the fields is given by the Gaussian distribution of Eq. (6). The convective derivative term describes a straight-line trajectory for constant velocity, the second derivative term in x allows for diffraction (wave-packet spreading), and the force term takes into account the spatially varying potential which affects only the final state.

It is assumed that the Raman fields are detuned far from resonance with the intermediate state so that coherent transitions from the initial state to the final state are dominant over incoherent optical pumping. In this case, the intermediate-state amplitude A_i can be adiabatically eliminated from Eqs. (9). Suppose that $\Omega_1 - \Omega_2 = \omega_{fi} = \omega_{fi} - \omega_{if}$ so that $\omega_{fi} - \Omega_1 = \omega_{if} - \Omega_2 \equiv -\Delta$. In the large-detuning limit, we have $\Delta \gg \gamma_i$, $\mathbf{q} \cdot \mathbf{v}$, Ω_{fi} , Ω_{if} , etc. Letting $A_i(t) = a_i(t) \exp(-i\Delta t)$ in Eqs. (9), the intermediate-state amplitude is approximately given by

$$\begin{aligned} A_i(t) &\simeq - \frac{\Omega_{fi}(\mathbf{R})}{2i \left[\frac{\gamma_i}{2} - i\Delta \right]} e^{i\mathbf{q} \cdot \mathbf{R} - i\Delta t} A_i(\mathbf{R}, t) \\ & \quad - \frac{\Omega_{if}(\mathbf{R})}{2i \left[\frac{\gamma_i}{2} - i\Delta \right]} e^{i\mathbf{q} \cdot \mathbf{R} - i\Delta t} A_f(\mathbf{R}, t). \quad (10) \end{aligned}$$

With Eq. (10), the evolution equations (9) for the initial- and final-state amplitudes take the form

$$\begin{aligned}
& \left[\frac{\partial}{\partial t} + \mathbf{v} \cdot \nabla - \frac{i\hbar}{2M} \frac{\partial^2}{\partial x^2} \right] A_i(\mathbf{R}, t) \\
&= - \frac{|\Omega_{if}(\mathbf{R})|^2}{4(\gamma_s/2 - i\Delta)} A_i - \frac{\Omega_{if}^*(\mathbf{R})\Omega_{if}(\mathbf{R})}{4 \left[\frac{\gamma_s}{2} - i\Delta \right]} A_f, \\
& \left[\frac{\partial}{\partial t} + \mathbf{v} \cdot \nabla - \frac{i\hbar}{2m} \frac{\partial^2}{\partial x^2} - \frac{i}{\hbar}(x - x_0)F \right] A_f(\mathbf{R}, t) \\
&= - \frac{|\Omega_{if}(\mathbf{R})|^2}{4 \left[\frac{\gamma_s}{2} - i\Delta \right]} A_f - \frac{\Omega_{if}(\mathbf{R})\Omega_{if}^*(\mathbf{R})}{4 \left[\frac{\gamma_s}{2} - i\Delta \right]} A_i.
\end{aligned} \quad (11)$$

Equations (11) are readily solved in perturbation

theory. This yields a spatial resolution function (see below) which includes the effects of both classical motion and diffraction of the moving atoms. In lowest order, the initial-state amplitude $A_i^{(0)}(y, x)$ can be taken to propagate neglecting the Raman fields. Further, the velocity will be taken to have only x and y components. It is assumed that the atomic distribution does not vary in the z direction. Then, the initial-state amplitude satisfies

$$\left[v_y \frac{\partial}{\partial y} + v_x \frac{\partial}{\partial x} - \frac{i\hbar}{2M} \frac{\partial^2}{\partial x^2} \right] A_i^{(0)}(y, x) = 0. \quad (12)$$

The solution to this equation is determined by free-particle propagation, where y/v_y plays the role of the time. If the amplitude A_i is specified in the plane located at y_1 along the atomic-beam axis, then the amplitude at an arbitrary position y_2, x_2 is evidently given by

$$A_i^{(0)}(y_2, x_2) = \int_{-\infty}^{\infty} dx_1' A_i(y_1, x_1') \int dk_1 \frac{1}{2\pi} e^{ik_1[x_2' - x_1' - v_x(y_2' - y_1)/v_y]} e^{-i(\hbar k_1^2/2m)(y_2' - y_1)/v_y}. \quad (13)$$

To lowest order in the Raman fields, the term on the right-hand side of the A_f evolution equation (11) proportional to A_f may be neglected, since A_f is assumed to be initially zero, prior to a Raman transition from state i . (That is, we neglect the light shift and optical pumping due to the weak nonresonant Raman fields. In practice, the Raman-field intensities are adjusted to give equal light shifts which cancel for the $i \rightarrow f$ transition.) The solution for the final-state amplitude in the y, x plane is then readily obtained by means of the Green's function which satisfies

$$\left[v_y \frac{\partial}{\partial y} + v_x \frac{\partial}{\partial x} - \frac{i\hbar}{2M} \frac{\partial^2}{\partial x^2} - i(x - x_0) \frac{F}{\hbar} \right] G_F(y, y_2'; x, x_2') = \delta(y - y_2') \delta(x - x_2'). \quad (14)$$

The final-state amplitude is given by

$$A_f(y, x) = \int dy_2' \int dx_2' G_F(y, y_2'; x, x_2') \frac{-\Omega_{if}(y_2')\Omega_{if}^*(y_2')}{4 \left[\frac{\gamma_s}{2} - i\Delta \right]} A_i^{(0)}(y_2', x_2'), \quad (15)$$

where the Rabi frequencies are taken to be Gaussian distributions centered at y_1 along the y axis [see Eq. (6)] but independent of x for simplicity (i.e., the measurement length is taken to be small compared to the radius and the Rayleigh length of the Raman beams).

As shown in Appendix A, the required Green's function for propagating in a uniform force field is obtainable by transforming to momentum space and is given by

$$\begin{aligned}
G_F(y, y_2'; x, x_2') &= \frac{\Theta(y - y_2')}{v_y} \int_{-\infty}^{\infty} dk \frac{1}{2\pi} \exp \left\{ ik \left[x - x_2' - v_x \frac{y - y_2'}{v_y} - \frac{F}{2M} \left(\frac{y - y_2'}{v_y} \right)^2 \right] \right\} e^{-i(\hbar k^2/2M)[(y - y_2')/v_y]} \\
&\times \exp \left[i \frac{F}{\hbar} \frac{y - y_2'}{v_y} (x - x_0) - i \frac{Fv_x}{2\hbar} \left(\frac{y - y_2'}{v_y} \right)^2 - i \frac{F^2}{6\hbar M} \left(\frac{y - y_2'}{v_y} \right)^3 \right].
\end{aligned} \quad (16)$$

In this form, the Green's function has a simple physical interpretation. Neglecting wave-packet spreading, integration over k for the first exponential factor yields a δ function requiring the atom to follow the classical trajectory during the time $(y - y_2')/v_y$. The second exponential takes wave-packet spreading into account. The last exponential factor is just the phase acquired by the final state of the atom in propagating through the classical path in the potential due to the force field.

In Appendix B, the integrated final-state flux emerging from the Raman region is evaluated starting from Eq. (15) and yields the following result:

$$\begin{aligned}
 & \int_{-\infty}^{\infty} dx |A_f(y, x)|^2 \\
 &= \left| \frac{\Omega_{fi} \Omega_{if}^*}{4v_y \left[\frac{\gamma_s}{2} - i\Delta \right]} \right|^2 \int dx'_1 \int_{-\infty}^{\infty} du_- \int_{-\infty}^{\infty} du_+ e^{-u_-^2/2d^2} e^{-(2u_+^2/d^2)} \\
 & \quad \times e^{-i[(Fv_x)/(\hbar v_y^2)]u_+ u_-} e^{-i[(F)/(\hbar v_y)](x'_1 - x_0)u_-} e^{-i[(F^2)/12\hbar M v_y^3]u_-^3} \\
 & \quad \times A_i \left[y_1, x'_1 - \frac{F}{2Mv_y^2} u_+ u_- \right] A_i^* \left[y_1, x'_1 + \frac{F}{2Mv_y^2} u_+ u_- \right]. \quad (17)
 \end{aligned}$$

Equation (17) gives the general result for the integrated flux in the final state in terms of an arbitrary initial-state amplitude specified at the center of the Raman region $y = y_1$, $A_i(y_1, x)$. To obtain the final-state count rate, this result must be multiplied by the atomic density, the atomic-beam velocity, and the transverse dimension of the atomic beam perpendicular to the measurement axis.

III. RESULTS

In the following sections, the spatial resolution obtained with the Raman-induced resonance imaging method is examined first, in order to verify the statements made in the Introduction based on heuristic arguments. Then, the final-state wave function is examined to determine the momentum and position distribution of the final-state atoms. For a plane-wave input in the initial state, it is shown that under appropriate circumstances, a minimum-uncertainty final-state wave packet may be obtained.

A. The spatial resolution function

Using the result given by Eq. (17), the spatially integrated final-state flux can be determined for any given spatially varying initial-state amplitude $A_i(y_1, x)$. This determines the dependence of the signal on the applied

uniform magnetic field (i.e., on the resonant point x_0). Further, in an important special case, described below, this result is to determine the general form of the sampling function which measures the incident atomic distribution in state i . We will refer to this sampling function as the resolution function.

The Gaussian factors in the integrand of Eq. (17) constrain u_{\pm} to distances of order d . If the initial-state amplitude does not vary over distances of order $(F/2M)(d/v_y)^2$, then the dependence of the amplitudes on u_{\pm} may be neglected. This requires that the interaction time d/v_y in the Raman fields be not too large, so that the final state does not accelerate over distances comparable to the length scale over which the initial-state amplitude varies. In this case, the u_+ integration is readily done and the integrated flux then takes the form

$$\begin{aligned}
 \int_{-\infty}^{\infty} dx |A_f(y, x)|^2 &= \left| \frac{\Omega_{fi} \Omega_{if}^* d \sqrt{\pi}}{\left[\frac{\gamma_s}{2} - i\Delta \right] 4v_y} \right|^2 \\
 & \quad \times \int dx'_1 R_1(x'_1 - x_0) \\
 & \quad \times |A_i(y_1, x'_1)|^2, \quad (18)
 \end{aligned}$$

where the resolution function R_1 is given by

$$R_1(x'_1 - x_0) = \int_{-\infty}^{\infty} du_- \frac{1}{(2\pi d^2)^{1/2}} \exp \left\{ - \left[\frac{1}{2d^2} + \frac{1}{8} \left(\frac{Fv_x d}{\hbar v_y^2} \right)^2 \right] u_-^2 \right\} \exp \left[-i \frac{F}{\hbar v_y} (x'_1 - x_0) u_- - i \frac{F^2}{12\hbar M v_y^3} u_-^3 \right]. \quad (19)$$

Physically, the meaning of this result is clear. The exponent in the Gaussian factor decreases as the Raman beam radius d is made larger and the interaction time longer, corresponding to higher-frequency resolution. This tends to increase the spatial resolution and narrow the resolution function. However, as d is increased, the motion along the measurement axis due to v_x tends to increase the exponent and broadens the resolution function. The acceleration of the final state leads to a phase factor in the integrand which is cubic in the time (u_-/v_y) , as one would expect using classical arguments. In addition,

diffraction also leads to a cubic time dependence of the phase.

This result can be cast in a simpler form by using the natural length scales for this problem which are discussed in the Introduction. The form of the resulting resolution function serves to justify the heuristic treatment of the resolution limits.

It is convenient to express distance along the measurement axis in units of the acceleration limited-resolution length, Eq. (4). The resolution length in turn leads to the natural unit of transit time across the Raman

region, T_0 . Using $(F/2M)T_0^2 = \Delta x_{\text{accel}}$ one obtains $T_0 = (2M\hbar/F^2)^{1/3}$. The corresponding unit of distance along the atomic-beam axis, y , is just $d_0 = v_y T_0$. Defining $u_- = \eta d_0$, and expressing $x'_1 - x_0$ in units of Δx_{accel} , the resolution function can be recast into the following form:

$$R_0(x'_1 - x_0) = \frac{1}{\Delta x_{\text{accel}}} I \left[\frac{x'_1 - x_0}{\Delta x_{\text{accel}}} \right], \quad (20)$$

where

$$I(s) = \int_{-\infty}^{\infty} d\eta \frac{1}{2\pi} e^{-\alpha(\eta^2/2)} e^{-i \text{sgn}(F)s\eta - i(\eta^3/6)} \\ = \int_0^{\infty} d\eta \frac{1}{\pi} e^{-\alpha(\eta^2/2)} \cos \left[\text{sgn}(F)s\eta + \frac{\eta^3}{6} \right], \quad (21)$$

with $\text{sgn}(F) = +1(-1)$ for a positive (negative) force. Note that $\int dx'_1 R_0(x'_1 - x_0) = 1$. The parameters appearing in Eq. (21) are given by

$$\alpha = \frac{d_0^2}{d^2} + \frac{d^2}{d_0^2} r^4, \\ r = \frac{\Delta x_{\text{vel}}}{\Delta x_{\text{accel}}}, \quad (22)$$

$$\Delta x_{\text{vel}} = \left[\frac{2\hbar v_x}{|F|} \right]^{1/2},$$

$$d_0 = v_y \left[\frac{2M\hbar}{F^2} \right]^{1/3}.$$

In terms of R_0 , the integrated final-state flux takes the form

$$\int_{-\infty}^{\infty} dx |A_f(y, x)|^2 \\ = \eta_R \frac{\sqrt{2\pi\hbar} v_y}{d|F|} \int dx' |A_i(y_1, x')|^2 R_0(x' - x_0) \\ \simeq \eta_R \frac{\sqrt{2\pi\hbar} v_y}{d|F|} |A_i(y_1, x' = x_0)|^2, \quad (23)$$

where the approximate result is valid if the resolution function is narrow compared to the length scales over which the atomic distribution varies. The Raman transition probability is given by

$$\eta_R = \left| \frac{\Omega_i \Omega_f^* d \sqrt{\pi}}{\left[\frac{\gamma_s}{2} - i\Delta \right] 4v_y} \right|^2. \quad (24)$$

Note that the factor which multiplies the Raman transition probability in Eq. (23) is of the order of the position resolution. The approximate result could, of course, have been written down on the basis of physical arguments, without detailed calculation. The important feature is

that the detailed shape of the resolution function is obtained.

According to Eqs. (20) and (21), the resolution function will be approximately Gaussian if the parameter α is large compared to unity, so that the cubic dependence of the phase on η can be neglected. When the velocity is so large that $\Delta x_{\text{vel}} > \Delta x_{\text{accel}}$, which implies $v_x > \hbar/2M\Delta x_{\text{accel}}$, the factor r^4 in α of Eq. (22) quickly becomes large and Gaussian dependence dominates the integrand. In this limit, the resolution function takes the form

$$I(s) = \frac{e^{-s^2/2\alpha}}{\sqrt{2\pi\alpha}}. \quad (25)$$

According to Eq. (22), the parameter α is minimized for a certain value of the Raman-region diameter d . Physically, the frequency resolution increases as d is increased. This tends to increase the position resolution. However, the velocity along the measurement axis v_x causes the position to move during the measurement. Hence, an optimum diameter exists. Differentiating α with respect to d , and setting the result equal to zero, one obtains $d_{\text{opt}} = d_0/r$ and $\alpha_{\text{opt}} = 2r^2$. The corresponding resolution function then is given by Eqs. (20) and (25) as

$$R_0(x'_1 - x_0) = \frac{\exp \left[- \left| \frac{x'_1 - x_0}{\Delta x_{\text{vel}}} \right|^2 \right]}{\Delta x_{\text{vel}} \sqrt{\pi}} \quad (26)$$

and $d_{\text{opt}} = (v_y/v_x) \Delta x_{\text{vel}}$. Physically, the atom travels a distance along the measurement axis just equal to the optimum resolution length during the transit time across the Raman region. Note that the neglect of $Fu_+ u_- / 2Mv_y^2$ in the argument of the initial amplitude A_i in Eq. (17) is justified if A_i varies slowly compared to $Fd_{\text{opt}}^2 / 2Mv_y^2 = \hbar/2Mv_x < \Delta x_{\text{accel}}$ in this limit.

In the opposite limit when $\Delta x_{\text{vel}} < \Delta x_{\text{accel}}$, i.e., when $v_x < \hbar/2M\Delta x_{\text{accel}}$, the ratio r is less than unity and the parameter $\alpha \simeq d_0^2/d^2$. Hence, as the Raman-region diameter d is increased to order d_0 or greater, α decreases, and the functions $I(s)$ and R_0 narrow. As $\alpha \rightarrow 0$, it is clear from the exact equation (21) for $I(s)$ that the natural length scale for s is unity, since the cubic phase plays the dominant role in the integrand. This corresponds to spatial resolution comparable to the acceleration length. The function $I(s)$ is plotted in Fig. 3 for various values of α .

When α is of order unity (1–2), the shape is nicely localized and is nearly Gaussian. However, if α is made small, corresponding to a large Raman-region diameter, the function $I(s)$ is asymmetric. It oscillates on one side and decays on the other. Physically, this is linked to the fact that for a positive force, the final-state amplitude created at x' to the left of the resonance position x_0 within a distance of order Δx_{accel} accelerates to the right and interferes with the amplitude created at x_0 . Hence, the resolution function oscillates on the left side of x_0 for a positive force. However, final-state amplitude created

for x' to the right of x_0 accelerates further to the right away from x_0 and hence does not interfere. Thus, the resolution function rapidly dies off on this side of x_0 for a positive force. This behavior is, of course, related to the wave function for penetration of a potential barrier which varies linearly in position, but is opposite to what one might expect because the final state is accelerated rather than the initial state.

B. Minimum-uncertainty spatial wave packets

The process of measuring the initial-state distribution via the Raman-induced resonance imaging method naturally creates the final-state spatial wave function in the form of a localized packet, since the $i \rightarrow f$ transition occurs in a highly localized spatial region. Hence, the method is well suited to the creation and study of spatial wave packets and it is of interest to determine the momentum and position spread of such a state. For this purpose, we assume for simplicity that the initial state takes the form of a plane wave with $A_i(y_1, x) = 1$. In this case, the final-state spatial wave function after the Raman region where $y > y_1$ can be evaluated starting from Eq. (B6). The x' integration is straightforward and yields the unnormalized state for an atom of initial velocity $v = \hbar k / M$ as $\psi_f(y, x) = e^{ik \cdot R} A_f(y, x)$. Choosing a normalization constant so that $\int_{-\infty}^{\infty} dx |\psi_f(y, x)|^2 = 1$ yields the final-state wave function in the form

$$\psi_f(y, x) = \left[\frac{2\pi d^2 \hbar v_y}{|F|d} \left| \frac{\pi}{2} \right|^{1/2} \right]^{-1/2} e^{ik \cdot R} \times \int_{-\infty}^{\infty} dy'_2 \exp \left[- \left| \frac{y'_2 - y_1}{d} \right|^2 \right] \exp \left[i \left\{ \frac{F}{\hbar} \frac{y - y'_2}{v_y} (x - x_0) - \frac{F v_x}{2\hbar} \left[\frac{y - y'_2}{v_y} \right]^2 - \frac{F^2}{6\hbar M} \left[\frac{y - y'_2}{v_y} \right]^3 \right\} \right]. \quad (27)$$

Using Eq. (27), the momentum spread of the final-state wave packet is readily evaluated, since differentiation with respect to x just differentiates the phase factors and evaluation of the expectation values then requires only Gaussian integrals. The momentum spread is found to be

$$(\Delta p)^2 \equiv \overline{p^2} - \bar{p}^2 = M^2 (\Delta v_x)^2 + \left[\frac{Fd}{2v_y} \right]^2, \quad (28)$$

where the first term arises from a thermal average over the transverse velocity spread and the spread in the longitudinal velocity v_y along the atomic beam is ignored for simplicity. For a supersonic atomic beam, this is a

$$(\Delta x)^2 \equiv \overline{x^2} - \bar{x}^2 = \left[\frac{\hbar v_y}{Fd} \right]^2 + \left[\frac{Fd^2}{2Mv_y^2} \right]^2 \left[\frac{3}{16} + \left[\frac{y - y_1}{d} \right]^2 \right] + (\Delta v_x)^2 \left[\frac{y - y_1}{v_y} \right]^2 + \frac{F \overline{v_x}}{M v_y^3} \frac{d^2 (y - y_1)}{4} + \overline{v_x^2} \frac{d^2}{4 v_y^2}, \quad (30)$$

where the overline on the v_x terms indicates a thermal average over the initial transverse velocity spread and the v_y spread is again ignored. For these equations to be valid, the observation point must be after the Raman region,

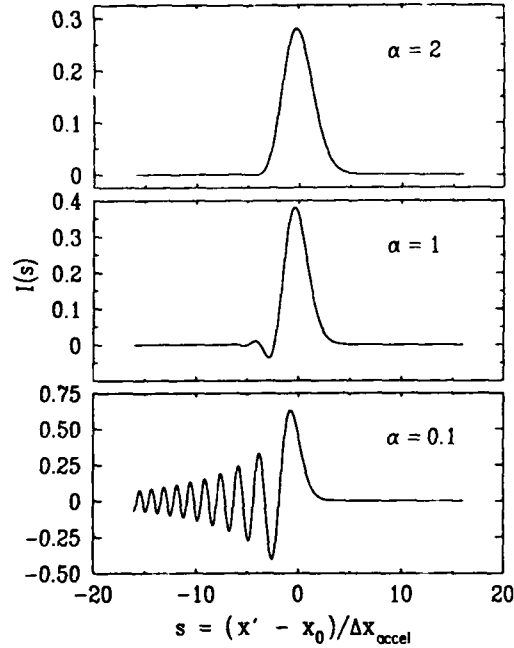


FIG. 3. Spatial resolution function. The s axis denotes position along the measurement axis in units of the optimum acceleration limited resolution length (see text).

reasonable approximation. With adequate beam collimation, the acceleration limit is attained and yields $(\Delta p)^2 = [(Fd)/2v_y]^2$.

The position spread also can be evaluated from Eq. (27) using integration by parts and the identity

$$\int_{-\infty}^{\infty} du u^n \exp i \left[\frac{F}{\hbar} \frac{y'_1 - y'_2}{v_y} u \right] = \frac{2\pi}{|F/\hbar v_y|} \left[\frac{-\hbar v_y}{iF} \frac{\partial}{\partial y'_2} \right]^n \delta(y'_2 - y'_1). \quad (29)$$

This yields

so that $y - y_1$ must be somewhat greater than d .

Using the position and momentum spread, the uncertainty product can be obtained. The most interesting case is that of high collimation where the spread in v_x

satisfies $\Delta v_x < \hbar/(M\Delta x_{\text{accel}})$ and the acceleration limit is achieved. In this case, the transverse coherence length of the incident beam is greater than Δx_{accel} and the force F imparts a momentum larger than the transverse thermal spread. Neglecting the transverse velocity spread terms, the uncertainty product then takes the form

$$(\Delta x)^2(\Delta p)^2 = \frac{\hbar^2}{4} \left[1 + \left(\frac{d}{d_0} \right)^6 \left[\frac{3}{16} + \left(\frac{y - y_1}{d} \right)^2 \right] \right], \quad (31)$$

where d_0 is the natural unit of distance along the atomic-beam axis in the acceleration limit, Eq. (22). For observation points not too far after the Raman region, $y - y_1$ is of the order of Raman region size d and Eq. (31) shows that a minimum uncertainty state is rapidly approached as the radius d is reduced somewhat below d_0 . Physically, this is easy to understand. When the radius d of the Raman region is reduced below the size d_0 which achieves optimum position resolution in the acceleration limit, atomic acceleration and diffraction during the transit time across the Raman region are negligible. In this case, the atom in its rest frame sees a Gaussian frequency pulse without chirping. Due to the linear spatial variation of the final-state potential, the Gaussian frequency distribution selects out a Gaussian spatial distribution for the final-state wave packet. This follows from Eq. (27) when the quadratic terms in the phase due to v_x and cubic terms due to the acceleration are neglected, which leads to a Gaussian spatial wave function for the final state.

IV. CONCLUSIONS

The calculation of the form of the resolution function and of the final-state wave function above justifies the statements made in Ref. 7 on the basis of heuristic arguments. The results for the ultimate spatial resolution Δx_{accel} show that very high spatial resolution is attainable for large spatially varying final-state level shifts. For example, a samarium atomic beam of nominal speed 6×10^4 cm/s in a level shift gradient of 10^{12} Hz/cm yields a spatial resolution ≈ 70 Å. To obtain this resolution, it is necessary that $\Delta x_{\text{vel}} < \Delta x_{\text{accel}}$ which is equivalent to $v_x < \hbar/(2M\Delta x_{\text{accel}})$. For the above conditions, this requires $v_x < 3$ cm/s corresponding to a beam collimation better than $50 \mu\text{m}$. The optimum Raman beam intensity $1/e$ radius d is about $140 \mu\text{m}$ in this case. Note that the Doppler shifts due to divergence of the Raman beams

cancel if the beam radii are matched at the focus.

For large spatially varying level shift gradients, the frequency resolution required to obtain the optimum spatial resolution is not as stringent as for small gradients. In this case, a simple one-photon transition may be applicable with long-lived excited states to achieve very high spatial resolution. For example, in ^{174}Yb , this method can be applied to excite the $^1S_0 \rightarrow ^3P_1$ transition and either absorption or resonance fluorescence in the interaction region can be directly measured by modulating the level shift gradient as done by Salomon *et al.*³ In this case, for suboptical wavelength spatial resolution the recoil momentum for a one-photon process will be negligible compared to the momentum imparted by the spatially varying potential.

An important application of the Raman-induced resonance imaging method is in the development of two-point correlation techniques. By employing two pairs of Raman difference frequencies, it is possible to access two separated spatial points with high spatial resolution. The final states for each of the regions can be made either identical or different so that the contribution of each region to the total detected signal can be made either distinguishable or indistinguishable. The use of two-point correlation measurements opens up the possibility of achieving the atomic analogue of the optical intensity correlations originally explored by Brown and Twiss. In this type of technique, only the transverse coherence length needs to be longer than the spatial separation between detection regions. This type of detection can be applied to perform atom antibunching experiments and is likely to be of use in studying atomic spatial coherence.

The simplicity of the proposed optical measurement methods suggests that experiments based on these techniques may be useful in studying quantum-mechanical features of atomic-position measurement in general.¹¹ Interesting applications include the creation and study of one-dimensional wave packets, which, as shown above, can be minimum-uncertainty Gaussian states under appropriate conditions. The evolution of position-squeezed states¹² also may be observable with one-dimensional harmonic wells based on spatially varying light-shift potentials.

ACKNOWLEDGMENTS

The author is indebted to George Welch and Jeff Gardner for many stimulating discussions and for carefully reading and commenting on the manuscript. This research is supported by Rome Air Development Center through Contract No. F19628-88-K-0012.

APPENDIX A. DERIVATION OF THE GREEN'S FUNCTION FOR PROPAGATION IN A UNIFORM FORCE FIELD

According to Eq. (14) of the text, the required Green's function satisfies

$$\left[v_y \frac{\partial}{\partial y} + v_x \frac{\partial}{\partial x} - \frac{i\hbar}{2M} \frac{\partial^2}{\partial x^2} - i(x - x_0) \frac{F}{\hbar} + \epsilon \right] G_F(y, y_2; x, x_2) = \delta(y - y_2) \delta(x - x_2), \quad (A1)$$

where a positive infinitesimal (ϵ) is added to the equation to ensure causality. The Green's function can be found by

Fourier-transform techniques. We begin by assuming the form

$$G(y, y'; x, x') = \int \int dk_y dk_x \frac{1}{(2\pi)^2} G(k_y, k_x) e^{i(k_y y + k_x x)}. \quad (\text{A2})$$

Substituting Eq. (A2) into Eq. (A1) yields

$$\begin{aligned} \int \int dk_y dk_x \frac{1}{(2\pi)^2} \left[ik_y v_y + ik_x v_x + \frac{i\hbar}{2M} k_x^2 + i \frac{F}{\hbar} x_0 + \epsilon \right] G(k_y, k_x) e^{i(k_y y + k_x x)} \\ - \frac{F}{\hbar} \int \int dk_y dk_x \frac{1}{(2\pi)^2} \left[\frac{\partial}{\partial k_x} e^{i(k_y y + k_x x)} \right] G(k_y, k_x) = \int \int dk_y dk_x \frac{1}{(2\pi)^2} e^{ik_y(y-y') + ik_x(x-x')}. \end{aligned} \quad (\text{A3})$$

The integral involving the derivative of the exponential, which arises from the x -dependent term in Eq. (A1), can be integrated by parts assuming $G(k_y, k_x = \pm\infty) = 0$. The surface terms then vanish, and the Fourier transform is found to satisfy

$$\frac{F}{\hbar} \frac{\partial G(k_y, k_x)}{\partial k_x} + i \left[k_y v_y + k_x v_x + \frac{\hbar}{2M} k_x^2 + \frac{F}{\hbar} x_0 - i\epsilon \right] G(k_y, k_x) = e^{-i(k_y y' + k_x x')}. \quad (\text{A4})$$

Note that the same equation is obtained by Fourier transforming Eq. (A1) with $\int \int dy dx \exp -i(k_y y + k_x x)$, provided that $G(y \rightarrow \pm\infty, x \rightarrow \pm\infty) \rightarrow 0$. This equation is readily solved using an integrating factor. Let (for $F \neq 0$)

$$G(k_y, k_x) = A(k_y, k_x) \exp \left[-i \frac{\hbar}{F} \int_a^{k_x} \left[k_y v_y + k'_x v_x + \frac{\hbar k_x'^2}{2M} + \frac{F}{\hbar} x_0 - i\epsilon \right] dk'_x \right], \quad (\text{A5})$$

where a is an undetermined constant. Then,

$$\frac{F}{\hbar} \frac{\partial A(k_y, k_x)}{\partial k_x} = \exp \left[i \frac{\hbar}{F} \int_a^{k_x} \left[k_y v_y + k'_x v_x + \frac{\hbar k_x'^2}{2M} + \frac{F}{\hbar} x_0 - i\epsilon \right] dk'_x \right] e^{-ik_y y' - ik_x x'}. \quad (\text{A6})$$

This has the solution

$$A(k_y, k_x) = \frac{\hbar}{F} \int_b^{k_x} dk_x'' \exp \left[i \frac{\hbar}{F} \int_a^{k_x''} \left[k_y v_y + k'_x v_x + \frac{\hbar k_x'^2}{2M} + \frac{F}{\hbar} x_0 - i\epsilon \right] dk'_x \right] e^{-ik_y y' - ik_x'' x'}. \quad (\text{A7})$$

Then

$$G(k_y, k_x) = \frac{\hbar}{F} \int_b^{k_x} dk_x'' e^{-ik_y y' - ik_x'' x'} \exp \left[-i \frac{\hbar}{F} \int_{k_x''}^{k_x} \left[k_y v_y + k'_x v_x + \frac{\hbar k_x'^2}{2M} + \frac{F}{\hbar} x_0 - i\epsilon \right] dk'_x \right], \quad (\text{A8})$$

where the constant a in Eq. (A5) drops out. As $k_x \rightarrow \infty$, $G(k_y, k_x) \rightarrow 0$ for positive F , since $\exp(-(\epsilon\hbar/F) \int_{k_x''}^{k_x} dk'_x) \rightarrow 0$. To ensure that $G(k_x \rightarrow -\infty) \rightarrow 0$, we must take $b = -\infty$. However, if $F < 0$, we need $b = +\infty$, so that $k_x'' > k_x$. Then, again as $k_x \rightarrow \pm\infty$, $G(k_y, k_x) \rightarrow 0$.

With Eqs. (A8) and (A2), the Green's function then takes the form

$$G(y, y'; x, x') = \int \int dk_y dk_x \frac{1}{(2\pi)^2} e^{ik_y(y-y') + ik_x x} \frac{\hbar}{F} \int_b^{k_x} dk_x'' e^{-ik_x'' x'} \exp \left[-i \frac{\hbar}{F} \int_{k_x''}^{k_x} \left[k_y v_y + k'_x v_x + \frac{\hbar k_x'^2}{2M} + \frac{F}{\hbar} x_0 \right] dk'_x \right]. \quad (\text{A9})$$

To incorporate the boundary conditions in an F -independent manner, it is convenient to change variables, letting $k_x = (F/\hbar)\tau$, $k_x' = (F/\hbar)\tau'$, and $k_x'' = (F/\hbar)\tau''$. Further, let $b'' = b/(F/\hbar)$. Note that if $F > 0$, $dk_x = |F/\hbar|d\tau$ and if $F < 0$, $dk_x = -|F/\hbar|d\tau$. In either case, $\int_{-\infty}^{\infty} dk_x \rightarrow |F/\hbar| \int_{-\infty}^{\infty} d\tau$, since the limits of integration change sign with the sign of F according to the above substitution. Then, with $\beta \equiv F/\hbar$, the Green's function takes the form

$$G(y, y'; x, x') = |\beta| \int_{-\infty}^{\infty} d\tau \frac{1}{2\pi} e^{i\beta\tau x} \int_{b''}^{\tau} d\tau'' e^{-i\beta\tau'' x'} \exp \left[-i \int_{\tau''}^{\tau} d\tau' \left[\beta\tau' v_x + \frac{\hbar\beta^2}{2M} \tau'^2 + \beta x_0 \right] \right] \int dk_y \frac{1}{2\pi} e^{ik_y[y-y'-v_y(\tau-\tau'')]} \quad (\text{A10})$$

The last factor is just $\delta(y - y' - v_y(\tau - \tau''))$. To ensure forward propagation, we want $G \rightarrow 0$ if $y < y'$. This requires $\tau > \tau''$. Hence, we take $b'' = -\infty$ independent of the sign of F . Then the Green's function becomes

$$G(y, y'; x, x') = |\beta| \int_{-\infty}^{\infty} d\tau \frac{1}{2\pi} e^{i\beta\tau x} \int_{-\infty}^{\tau} d\tau' e^{-i\beta\tau' x'} \exp \left[-i \int_{\tau'}^{\tau} d\tau'' \left(\beta\tau'' v_x + \frac{\hbar\beta^2}{2M} \tau''^2 + \beta x_0 \right) \right] \delta(y - y' - v_y(\tau - \tau')) . \quad (\text{A11})$$

By construction, $\tau > \tau'$, so that the δ function in Eq. (A11) is zero unless $y > y'$. In this case, the τ'' integration is readily carried out to obtain

$$G(y, y'; x, x') = \Theta(y - y') \frac{|\beta|}{v_y} \int_{-\infty}^{\infty} d\tau \exp \left[i\beta\tau x - i\beta \left[\tau - \frac{y - y'}{v_y} \right] x' \right] \exp \left[-i \int_{\tau - (y - y')/v_y}^{\tau} d\tau' \left(\beta\tau' v_x + \frac{\hbar\beta^2}{2M} \tau'^2 + \beta x_0 \right) \right] . \quad (\text{A12})$$

The τ' integration in the phase is then carried out and yields

$$G(y, y'; x, x') = \Theta(y - y') \frac{|\beta|}{v_y} \int_{-\infty}^{\infty} d\tau \frac{1}{2\pi} \exp \left[i\beta\tau(x - x') + i\beta \frac{y - y'}{v_y} x' \right] e^{i\phi(\tau)} , \quad (\text{A13})$$

where the phase ϕ is given by

$$\phi(\tau) = -\beta v_x \tau \frac{y - y'}{v_y} + \frac{\beta v_x}{2} \left[\frac{y - y'}{v_y} \right]^2 - \beta x_0 \frac{y - y'}{v_y} - \frac{\hbar\beta^2}{2M} \tau^2 \frac{y - y'}{v_y} + \frac{\hbar\beta^2}{2M} \tau \left[\frac{y - y'}{v_y} \right]^2 - \frac{\hbar\beta^2}{6M} \left[\frac{y - y'}{v_y} \right]^3 . \quad (\text{A14})$$

It is convenient to make the substitution $k = \beta\tau$ in Eq. (A13). In this case, for $\beta > 0$, $\int_{-\infty}^{\infty} d\tau \rightarrow \int_{-\infty}^{\infty} dk / |\beta|$. For $\beta < 0$, $\int_{-\infty}^{\infty} d\tau \rightarrow \int_{\infty}^{-\infty} -dk / |\beta| = \int_{-\infty}^{\infty} dk / |\beta|$. The Green's function is then given by

$$G(y, y'; x, x') = \frac{\Theta(y - y')}{v_y} \int_{-\infty}^{\infty} dk \frac{1}{2\pi} \exp \left[ik \left[x - x' - v_x \frac{y - y'}{v_y} \right] \right] \exp \left[-i \frac{\hbar k^2}{2M} \frac{y - y'}{v_y} - i \frac{\hbar\beta}{2M} k \left[\frac{y - y'}{v_y} \right]^2 \right] \\ \times \exp \left[i\beta \frac{y - y'}{v_y} (x' - x_0) + i \frac{\beta v_x}{2} \left[\frac{y - y'}{v_y} \right]^2 - i \frac{\hbar\beta^2}{6M} \left[\frac{y - y'}{v_y} \right]^3 \right] . \quad (\text{A15})$$

The form of Eq. (A15) can be improved somewhat by noting that in propagating the final-state amplitude, the integration over x' projects out the plane-wave component of wave vector k' , where k' is the coefficient of $-x'$ in the phase which appears in the integrand above. With the substitution $k' = k - \beta[(y - y')/v_y]$, k may be eliminated in favor of the integration variable k' . Then, eliminating the $(')$ and using $\hbar\beta = F$, one obtains

$$G_F(y, y'_2; x, x'_2) = \frac{\Theta(y - y'_2)}{v_y} \int_{-\infty}^{\infty} dk \frac{1}{2\pi} \exp \left[ik \left[x - x'_2 - v_x \frac{y - y'_2}{v_y} - \frac{F}{2M} \left[\frac{y - y'_2}{v_y} \right]^2 \right] \right] \exp \left[-i \frac{\hbar k^2}{2M} \frac{y - y'_2}{v_y} \right] \\ \times \exp \left[i \frac{F}{\hbar} \frac{y - y'_2}{v_y} (x - x_0) - i \frac{F v_x}{2\hbar} \left[\frac{y - y'_2}{v_y} \right]^2 - i \frac{F^2}{6\hbar M} \left[\frac{y - y'_2}{v_y} \right]^3 \right] , \quad (\text{A16})$$

which is identical to the Green's function given in Eq. (16) of the text.

APPENDIX B: DERIVATION OF THE INTEGRATED FINAL-STATE FLUX

To proceed, it is convenient to perform the x'_2 integration in Eq. (15) first. From Eqs. (13) and (15) this requires evaluation of the integral

$$I \equiv \int dx'_2 G_F(y, y'_2; x, x'_2) \exp \left[ik_1 \left[x'_2 - x'_1 - v_x \frac{y'_2 - y_1}{v_y} \right] \right] \exp \left[-i \frac{\hbar k_1^2}{2M} \frac{y'_2 - y_1}{v_y} \right] . \quad (\text{B1})$$

Using

$$\int dx'_2 \frac{1}{2\pi} e^{i(k_1 - k)x'_2} = \delta(k - k_1) \quad (\text{B2})$$

yields

$$\begin{aligned} I = & \frac{\Theta(y - y'_2)}{v_y} \exp \left\{ ik_1 \left[x - x'_1 - v_x \frac{y - y_1}{v_y} - \frac{F}{2M} \left(\frac{y - y'_2}{v_y} \right)^2 \right] \right\} \exp \left[-i \frac{\hbar k_1^2}{2M} \frac{y - y_1}{v_y} \right] \\ & \times \exp \left[-\frac{F}{\hbar} \frac{y - y'_2}{v_y} (x - x_0) - i \frac{F v_x}{2\hbar} \left(\frac{y - y'_2}{v_y} \right)^2 - i \frac{F^2}{6\hbar M} \left(\frac{y - y'_2}{v_y} \right)^3 \right]. \end{aligned} \quad (\text{B3})$$

The k_1 integration required by Eqs. (15), (B3), and (13) is done next. This requires evaluation of the integral

$$I_1 = \int dk_1 \frac{1}{2\pi} \exp \left\{ ik_1 \left[x - x'_1 - v_x \frac{y - y_1}{v_y} - \frac{F}{2M} \left(\frac{y - y'_2}{v_y} \right)^2 \right] \right\} \exp \left[-i \frac{\hbar k_1^2}{2M} \frac{y - y_1}{v_y} \right] \quad (\text{B4})$$

$$= \frac{\sqrt{\pi}}{2\pi} \exp \left\{ +i \frac{M v_y}{2\hbar(y - y_1)} \left[x - x'_1 - v_x \frac{y - y_1}{v_y} - \frac{F}{2M} \left(\frac{y - y'_2}{v_y} \right)^2 \right]^2 \right\} / \left[\frac{i\hbar}{2M} \frac{y - y_1}{v_y} \right]^{1/2}, \quad (\text{B5})$$

where the observation point y is chosen downstream from the Raman region such that $y - y_1 \gg d$, and d is the radius of the Raman region. Since the Gaussian shape of the Raman regions constrains $y'_2 \approx y_1$ to within a distance d , the Θ function which appears in G_F can be taken equal to unity and the y'_2 integration region formally extended to infinity. With this result the final-state amplitude takes the form

$$\begin{aligned} A_f(y, x) = & - \frac{\Omega_H \Omega_f^*}{4v_y \left[\frac{\gamma_s}{2} - i\Delta \right]} \int dx'_1 A_i(y_1, x'_1) \\ & \times \int_{-\infty}^{\infty} dy'_2 \exp \left[-\left(\frac{y'_2 - y_1}{d} \right)^2 \right] \\ & \times \exp \left[i \frac{F}{\hbar} \frac{y - y'_2}{v_y} (x - x_0) - i \frac{F v_x}{2\hbar} \left(\frac{y - y'_2}{v_y} \right)^2 - i \frac{F^2}{6\hbar M} \left(\frac{y - y'_2}{v_y} \right)^3 \right] \\ & \times \frac{\sqrt{\pi}}{2\pi} \exp \left\{ +i \frac{M v_y}{2\hbar(y - y_1)} \left[x - x'_1 - v_x \frac{y - y_1}{v_y} - \frac{F}{2M} \left(\frac{y - y'_2}{v_y} \right)^2 \right]^2 \right\} / \left[\frac{i\hbar}{2M} \frac{y - y_1}{v_y} \right]^{1/2}, \end{aligned} \quad (\text{B6})$$

where the Rabi frequencies are evaluated at the peak of the Gaussian field distributions.

Our goal is to calculate the spatially integrated final-state flux at large distance downstream from the Raman region. The final-state atomic flux is proportional to $J = v_y |A_f(y, x)|^2$ for the case of a collimated atomic beam. The total signal is then $\dot{N} \propto \int \int dz dx J$, where the integrals extend across the atomic beam from $-\infty$ to ∞ . In order to take the limit $y - y_1 \rightarrow \infty$ when the observation point is well outside the Raman region, it is necessary to do the infinite x - z integration *before* taking the large- y limit. In this way, all of the flux is included at each value of y . Since the amplitude is z independent, only the x integral need be explicitly done. Using dummy integration variables x'_1, y'_2 and x''_1, y''_2 for the final-state amplitude given in Eq. (B6) and its complex conjugate, the required integral is given by

$$\begin{aligned}
\int_{-\infty}^{\infty} |A_f(y, x)|^2 dx = & \left| \frac{\Omega_{If} \Omega_{If}^*}{4v_y \left[\frac{\gamma_s}{2} - i\Delta \right]} \right|^2 \int dx'_1 \int dx''_1 A_i(y_1, x'_1) A_i^*(y_1, x''_1) \\
& \times \frac{1}{4\pi} \int_{-\infty}^{\infty} dx \frac{\exp \left\{ i \frac{Mv_y}{2\hbar(y-y_1)} \left[\left(x - x'_1 - v_x \frac{y-y_1}{v_y} \right)^2 - \left(x - x''_1 - v_x \frac{y-y_1}{v_y} \right)^2 \right] \right\}}{\frac{\hbar}{2M} \left| \frac{y-y_1}{v_y} \right|} \\
& \times \int_{-\infty}^{\infty} \int_{-\infty}^{\infty} dy'_2 dy''_2 \exp \left[-\frac{(y'_2 - y_1)^2 + (y''_2 - y_1)^2}{d^2} \right] \exp \left\{ i \frac{F}{\hbar} \frac{y'_2 - y''_2}{v_y} (x - x_0) \right\} \\
& \times \exp \left\{ i \frac{Mv_y}{2\hbar(y-y_1)} \left[\left(\frac{F}{2M} \left[\frac{y-y'_2}{v_y} \right]^2 \right)^2 - \left(\frac{F}{2M} \left[\frac{y-y''_2}{v_y} \right]^2 \right)^2 \right] \right\} \\
& \times \exp \left\{ -i \frac{Mv_y}{2\hbar(y-y_1)} 2 \frac{F}{2M} \left[(x - x'_1) \left[\frac{y-y'_2}{v_y} \right]^2 - (x - x''_1) \left[\frac{y-y''_2}{v_y} \right]^2 \right] \right\} \\
& \times \exp \left\{ -i \frac{F^2}{6\hbar M} \left[\left[\frac{y-y'_2}{v_y} \right]^3 - \left[\frac{y-y''_2}{v_y} \right]^3 \right] \right\}. \quad (B7)
\end{aligned}$$

Note that the two terms proportional to $(Fv_x/2\hbar)[(y-y'_2)/v_y]^2$ cancel in Eq. (B6), and hence do not appear in Eq. (B7).

At this point, the x integration is straightforward. We begin by rewriting Eq. (B7) in the form

$$\begin{aligned}
\int_{-\infty}^{\infty} |A_f(y, x)|^2 dx = & \left| \frac{\Omega_{If} \Omega_{If}^*}{4v_y \left[\frac{\gamma_s}{2} - i\Delta \right]} \right|^2 \int dx'_1 \int dx''_1 A_i(y_1, x'_1) A_i^*(y_1, x''_1) \\
& \times \int_{-\infty}^{\infty} \int_{-\infty}^{\infty} dy'_2 dy''_2 \exp \left[-\frac{(y'_2 - y_1)^2 + (y''_2 - y_1)^2}{d^2} \right] \exp \left[-i \frac{F}{\hbar} \frac{y'_2 - y''_2}{v_y} x_0 \right] \\
& \times \exp \left[i \frac{F^2[(y-y'_2)^4 - (y-y''_2)^4]}{8\hbar M v_y^3 (y-y_1)} \right] \exp \left[-i \frac{F^2[(y-y'_2)^3 - (y-y''_2)^3]}{6\hbar M v_y^3} \right] \\
& \times \exp \left[i \frac{F[x'_1(y-y'_2)^2 - x''_1(y-y''_2)^2]}{2\hbar v_y (y-y_1)} \right] \\
& \times \exp \left\{ i \frac{Mv_y}{2\hbar(y-y_1)} \left[\left(x'_1 + v_x \frac{y-y_1}{v_y} \right)^2 - \left(x''_1 + v_x \frac{y-y_1}{v_y} \right)^2 \right] \right\} I_x, \quad (B8)
\end{aligned}$$

where

$$\begin{aligned}
I_x = & \frac{1}{4\pi \frac{\hbar}{2M} \left| \frac{y-y_1}{v_y} \right|} \int_{-\infty}^{\infty} dx \exp \left[ix \left\{ \frac{F(y'_2 - y''_2)}{\hbar v_y} - \frac{Mv_y(x'_1 - x''_1)}{\hbar(y-y_1)} - \frac{F[(y-y'_2)^2 - (y-y''_2)^2]}{2\hbar v_y (y-y_1)} \right\} \right] \\
= & \delta(x'_1 - x''_1 + \epsilon) \quad (B9)
\end{aligned}$$

and

$$\epsilon(y'_2, y''_2) = \frac{F}{2Mv_y^2} [(y'_2 - y_1)^2 - (y''_2 - y_1)^2]. \quad (B10)$$

With Eqs. (B8) and (B9), one obtains

$$\begin{aligned}
 \int_{-\infty}^{\infty} |A_f(y, x)|^2 dx = & \left| \frac{\Omega_R \Omega_{If}^*}{4v_y \left[\frac{\gamma_s}{2} - i\Delta \right]} \right|^2 \int_{-\infty}^{\infty} \int_{-\infty}^{\infty} dy'_2 dy''_2 \exp \left[-\frac{(y'_2 - y_1)^2 + (y''_2 - y_1)^2}{d^2} \right] \\
 & \times \exp \left[-i \frac{F}{\hbar} \frac{y'_2 - y''_2}{v_y} x_0 \right] \exp \left[i \frac{F^2}{\hbar M v_y^3} \left[\frac{[(y - y'_2)^4 - (y - y''_2)^4]}{8(y - y_1)} - \frac{[(y - y'_2)^3 - (y - y''_2)^3]}{6} \right] \right] \\
 & \times \int dx'_1 A_i(y_1, x'_1) A_i^*(y_1, x'_1 - \epsilon) \exp \left[i \frac{F[x'_1(y - y'_2)^2 - (x'_1 - \epsilon)(y - y''_2)^2]}{2\hbar v_y(y - y_1)} \right] \\
 & \times \exp \left[i M v_y \left[2\epsilon \left[x'_1 + v_x \frac{y - y_1}{v_y} \right] - \epsilon^2 \right] / 2\hbar(y - y_1) \right]. \quad (B11)
 \end{aligned}$$

In order to display explicitly the reality of the right-hand side of Eq. (B11), it is convenient to make the substitution $x'_1 \rightarrow x'_1 + (\epsilon/2)$. Equation (B11) then takes the form

$$\begin{aligned}
 \int_{-\infty}^{\infty} |A_f(y, x)|^2 dx = & \left| \frac{\Omega_R \Omega_{If}^*}{4v_y \left[\frac{\gamma_s}{2} - i\Delta \right]} \right|^2 \int_{-\infty}^{\infty} \int_{-\infty}^{\infty} dy'_2 dy''_2 \exp \left[-\frac{(y'_2 - y_1)^2 + (y''_2 - y_1)^2}{d^2} \right] \\
 & \times \int dx'_1 A_i \left[y_1, x'_1 + \frac{\epsilon}{2} \right] A_i^* \left[y_1, x'_1 - \frac{\epsilon}{2} \right] e^{i\phi(y'_2, y''_2, x'_1)}, \quad (B12)
 \end{aligned}$$

where

$$\begin{aligned}
 \phi(y'_2, y''_2, x'_1) = & \frac{F}{\hbar v_y} (y'_2 - y''_2) x_0 + \frac{F^2}{\hbar M v_y^3} \left[\frac{[(y - y'_2)^4 - (y - y''_2)^4]}{8(y - y_1)} - \frac{[(y - y'_2)^3 - (y - y''_2)^3]}{6} \right] \\
 & + \frac{F x'_1 [(y - y'_2)^2 - (y - y''_2)^2]}{2\hbar v_y (y - y_1)} + \frac{F}{2\hbar v_y (y - y_1)} \frac{\epsilon}{2} [(y - y'_2)^2 + (y - y''_2)^2] \\
 & + \frac{M v_y}{\hbar (y - y_1)} \left[x'_1 + v_x \frac{y - y_1}{v_y} \right] \epsilon. \quad (B13)
 \end{aligned}$$

Note that the right-hand side is invariant under complex conjugation if the substitution $y'_2 \leftrightarrow y''_2$ is made (ϵ changes sign).

Next, we take advantage of the fact that the observation point y is chosen downstream from the Raman region at y_1 , such that $y - y_1 \gg y'_2 - y_1 \approx d$. In this case, it is convenient to make the substitution $u_1 = y'_2 - y_1$ and $u_2 = y''_2 - y_1$. Then, $(y - y'_2)^n - (y - y''_2)^n$, which appears in the phase ϕ can be written in the form $(y - y_1 - u_1)^n - (y - y_1 - u_2)^n$ and expanded exactly in powers of $(y - y_1) \gg u_i \approx d$. Hence,

$$\begin{aligned}
 (y - y'_2)^4 - (y - y''_2)^4 &= -4(y - y_1)^3(u_1 - u_2) + 6(y - y_1)^2(u_1^2 - u_2^2) \\
 &\quad - 4(y - y_1)(u_1^3 - u_2^3) + u_1^4 - u_2^4, \\
 (y - y'_2)^3 - (y - y''_2)^3 &= -3(y - y_1)^2(u_1 - u_2) + 3(y - y_1)(u_1^2 - u_2^2) \\
 &\quad - u_1^3 + u_2^3,
 \end{aligned}$$

$$(y - y'_2)^2 - (y - y''_2)^2 = -2(y - y_1)(u_1 - u_2) + u_1^2 - u_2^2, \quad (B14)$$

$$\begin{aligned}
 (y - y'_2)^2 + (y - y''_2)^2 &= 2(y - y_1)^2 - 2(y - y_1)(u_1 + u_2) + u_1^2 + u_2^2, \\
 \epsilon &= \frac{F}{2M v_y^2} (u_2^2 - u_1^2).
 \end{aligned}$$

These results are substituted into Eq. (B13) and terms are collected which are proportional to $(y - y_1)^n$ where n runs from +2 to -1. It is found that all terms vanish except for the one with $n = 0$. The phase then takes the form

$$\begin{aligned}
 \phi(u_1, u_2, x'_1) = & -\frac{F}{\hbar v_y} (u_1 - u_2)(x'_1 - x_0) \\
 & - \frac{F v_x}{2\hbar v_y^2} (u_1^2 - u_2^2) \\
 & - \frac{F^2}{12\hbar M v_y^3} (u_1 - u_2)^3. \quad (B15)
 \end{aligned}$$

The phase does not depend on the distance from the Raman region y_1 to the observation point y . This is reasonable, since the integrated flux at observation points well outside the Raman region ($y - y_1 \gg d$) should be independent of the observation position even when

diffraction and acceleration are present. Note that the phase does not separate into two terms which are functions of u_1 and u_2 due to the cubic dependence on $u_1 - u_2$. With Eq. (B15), the integrated final-state flux is given by

$$\int_{-\infty}^{\infty} dx |A_f(y, x)|^2 = \left| \frac{\Omega_{fi} \Omega_{if}^*}{4v_y \left[\frac{\gamma_s}{2} - i\Delta \right]} \right|^2 \int dx'_1 \int_{-\infty}^{\infty} du_1 \int_{-\infty}^{\infty} du_2 \exp \left[-\frac{u_1^2 + u_2^2}{d^2} \right] \\ \times \exp \left[-i \left[\frac{F}{\hbar v_y} (u_1 - u_2)(x'_1 - x_0) + \frac{Fv_x}{2\hbar v_y^2} (u_1^2 - u_2^2) + \frac{F^2}{12\hbar M v_y^3} (u_1 - u_2)^3 \right] \right] \\ \times A_i \left[y_1, x'_1 + \frac{\epsilon}{2} \right] A_i^* \left[y_1, x'_1 - \frac{\epsilon}{2} \right], \quad (\text{B16})$$

where $\epsilon(u_1, u_2)$ is given in Eq. (B14).

Since the phase Eq. (B16) is dependent principally on the difference between u_1 and u_2 it is convenient to make the variable change $u_+ \equiv (u_1 + u_2)/2$ and $u_- = u_1 - u_2$. In this case, the Jacobian of the transformation is unity so that $du_1 du_2 = du_+ du_-$. Integration is over the entire plane. Substituting $u_1 = u_+ + (u_-/2)$ and $u_2 = u_+ - (u_-/2)$ into Eq. (B16), one obtains

$$\int_{-\infty}^{\infty} dx |A_f(y, x)|^2 = \left| \frac{\Omega_{fi} \Omega_{if}^*}{4v_y \left[\frac{\gamma_s}{2} - i\Delta \right]} \right|^2 \int dx'_1 \int_{-\infty}^{\infty} du_- \int_{-\infty}^{\infty} du_+ \exp \left[-\frac{u_-^2}{2d^2} \right] \exp \left[-\frac{2u_+^2}{d^2} \right] \\ \times \exp \left[-i \frac{Fv_x}{\hbar v_y^2} u_+ u_- \right] \exp \left[-i \frac{F}{\hbar v_y} (x'_1 - x_0) u_- - i \frac{F^2}{12\hbar M v_y^3} u_-^3 \right] \\ \times A_i \left[y_1, x'_1 - \frac{F}{2M v_y^2} u_+ u_- \right] A_i^* \left[y_1, x'_1 + \frac{F}{2M v_y^2} u_+ u_- \right]. \quad (\text{B17})$$

Equation (B17) gives the general result for the integrated flux in the final state in terms of the initial-state amplitude.

¹See P. E. Martin, B. G. Oldaker, A. H. Miklich, and D. E. Pritchard, Phys. Rev. Lett. **60**, 515 (1988), and references therein.

²V. P. Chebotayev, B. Ya. Dubetsky, A. P. Kasantsev, and V. P. Yakovlev, J. Opt. Soc. Am. B **2**, 1791 (1985).

³C. Salomon, J. Dalibard, A. Aspect, H. Metcalf, and C. Cohen-Tannoudji, Phys. Rev. Lett. **59**, 1659 (1987).

⁴V. I. Balykin and V. S. Letokhov, Phys. Today **42** (4), 23 (1989).

⁵A. Aspect, E. Arimondo, R. Kaiser, N. Vansteenkiste, and C. Cohen-Tannoudji, Phys. Rev. Lett. **61**, 826 (1988).

⁶See, for example, W. D. Phillips, J. V. Prodan, and H. J.

Metcalf, J. Opt. Soc. Am. B **2**, 1751 (1985).

⁷J. E. Thomas, Opt. Lett. **14**, 1186 (1989).

⁸See A. Anderson, S. Haroche, E. Hinds, W. Jhe, and D. Meshede, Phys. Rev. A **37**, 3597 (1988).

⁹See J. A. Yeazell, M. Mallalieu, and C. R. Stroud, Jr., Phys. Rev. Lett. **64**, 2007 (1990), and references therein.

¹⁰J. E. Thomas, P. R. Hemmer, S. Ezekiel, C. C. Leiby, Jr., R. H. Picard, and C. R. Willis, Phys. Rev. Lett. **48**, 867 (1982).

¹¹M. Ozawa, Phys. Rev. A **41**, 1735 (1990).

¹²H. P. Huen, Phys. Rev. Lett. **51**, 719 (1983).

**MISSION
OF
ROME LABORATORY**

Rome Laboratory plans and executes an interdisciplinary program in research, development, test, and technology transition in support of Air Force Command, Control, Communications and Intelligence (C³I) activities for all Air Force platforms. It also executes selected acquisition programs in several areas of expertise. Technical and engineering support within areas of competence is provided to ESD Program Offices (POs) and other ESD elements to perform effective acquisition of C³I systems. In addition, Rome Laboratory's technology supports other AFSC Product Divisions, the Air Force user community, and other DOD and non-DOD agencies. Rome Laboratory maintains technical competence and research programs in areas including, but not limited to, communications, command and control, battle management, intelligence information processing, computational sciences and software producibility, wide area surveillance/sensors, signal processing, solid state sciences, photonics, electromagnetic technology, superconductivity, and electronic reliability/maintainability and testability.